



**HEALTH MONITORING OF AIRCRAFT
BY NONLINEAR ELASTIC WAVE SPECTROSCOPY**

AERONEWS

EC SIXTH FRAMEWORK PROGRAMME
PRIORITY 4: AERONAUTICS AND SPACE

SPECIFIC TARGETED RESEARCH: AST3-CT-2003-502927

PROJECT WEBPAGE: <http://www.kuleuven-kortrijk.be/aeronews/>

PROJECT COORDINATOR: Prof. [KOEN VAN DEN ABEELE](#)



Deliverable D7

A new theoretical approach and a methodology on how to locate/image defects or damaged regions using NEWS techniques in simple objects, including preliminary tests of the imaging approach to specially manufactured samples

Period covered: from March 1, 2004 to February 29, 2008

Date of preparation: April 15, 2006

Update: April 15, 2008

Start date of project: March 1, 2004 Duration: 4 years (February 29, 2008)

Project coordinator name: Koen Van Den Abeele

Project coordinator organization name: KULeuven

Report authors: Polito, CU, GIP-U, KULeuven, IZFP, UNIVBRIS

Final version (confidential)

Introduction

Improvement of NEWS techniques can lead to a significant breakthrough in the development of new reliable and robust damage imaging systems. However, extensive theoretical studies and numerical modelling are required in order to aid the design, application and optimisation of these methodologies. To achieve these objectives, Work-Package 2 focused on (i) the development of theoretical and numerical models to simulate damage types identified in WP1, and (ii) the development of algorithms which enabled the detection of defective zones in large scale structures, localising faults and predicting their impact using NEWS measurements.

The ultimate goal of WP2 was to support experimental procedures and methodologies, providing guidance in terms of method selection, placement of sensors and actuators, and data acquisition and processing, assisting Work-Packages WP1, WP3 and WP4.

Two sub-packages were distinguished in WP2: Pure and applied modelling.

WP2.1: Simulation Studies of damaged simple and complex components;

WP2.2: Damage localization procedure and NEWIMAGE.

The objective for Deliverable D7 is to report –within WP2.2– on the development of damage localization procedures as an extension to NEWS methods based on numerical experiments

In this respect the following tasks have been performed in Work-Package 2 (WP2.2):

- Development of direct algorithms to interrogate isolated parts within larger structures.
- Development of indirect algorithms to identify damage location, magnitude and typologies using inverse modelling techniques
- Design of a one- two- and three-dimensional damage imaging technique called NEWIMAGE.
- Model updating by verification and validation of the localization procedures on samples with known (e.g. visible laser induced) internal cracks and comparison with other methods.

This final report on Deliverable D7 contains 3 parts:

- D7.1 a description of two possible methodologies for damage localization and imaging
- D7.2 a sensitivity study of the influence of the sample geometry on the phases in a nonlinear transmission experiment for bond quality characterization
- D7.3 imaging using the vibro-acoustics methods

D7.1. Damage localisation and imaging methodologies

In the framework of WP2.2 the Partners have developed different techniques for damage localization and imaging. In particular, efforts have been focused on two techniques:

- (a) MuMoNRAS: MultiMode Nonlinear Resonant Ultrasound Spectroscopy (1D)
- (b) NEWS based TR: Time Reversed elasticity based on Nonlinear Elastic Wave Spectroscopy (2D-3D)

(1a) MuMoNRAS (Multi Mode Nonlinear Resonance Acoustic Spectroscopy)

KULeuven and POLITO developed the methodology and applications for damage localization using MuMoNRAS. The methodology is based on the interpretation of the resonance frequency shift for different resonance modes of a given object in terms of the corresponding stress field of the resonance mode.

We give here the one-dimensional version, which can be extended to more dimensions in a straightforward manner.

Assume a 1D system which we will drive longitudinally at one end. If the system contains microdamage (nonlinearity), either globally or localized, we can examine the nonlinear resonance response of the object near several of its resonance frequencies. KULeuven¹ developed an analytical model for this situation (only pure hysteretic nonlinearity) and found that for a localized damage centred at $x=x_c$, extending from $[x_c-w/2, x_c+w/2]$ (with $w \ll L$) the resonance frequency shift is given as:

$$\begin{aligned} \Omega_{res,Local}(A_m) &\approx \Omega_{res}(0) \left[1 - \frac{\alpha w}{L} \left(1 + \frac{4}{3\pi Q} \right) \left| \sin^3 \left(m \frac{\pi}{L} x_c \right) \right| \varepsilon_m \right] \\ &\approx \Omega_{res}(0) [1 - \Theta_m(\alpha, w, x_c) \varepsilon_m] \end{aligned}$$

Here, $\Omega_{res}(0)$ denotes the ‘linear’ or ‘low amplitude’ resonance frequency, Q the quality factor (inverse attenuation), ε_m the strain response amplitude of mode m at resonance due to an excitation amplitude A_m , and α the constant hysteretic nonlinearity in the localized

¹ K. Van Den Abeele and F. Windels, “Characterisation and imaging of microdamage using Nonlinear Resonance Ultrasound Spectroscopy (NRUS): An analytical model”, in *"The universality of nonclassical nonlinearity, with applications to NDE and Ultrasonics"*, Ed. P.P. Delsanto, Springer, , NewYork, Chapter 23, pp. 369-388 (2006)

zone. In a hysteretic system the relative change in the resonance frequency, for any resonance mode, is proportional to the strain response amplitude of this mode. The proportionality coefficient is given by Θ_m , which depends on the strength, the extent and the location of the damage (see also the reported results on nonlinear resonance in Deliverable D6). Since α is connected to the hysteretic strength γ ($\alpha = \gamma K_0^2 = \frac{\hat{\gamma}}{N} K_0^2$ and by consequence a positive parameter), the relative change in the resonance frequency will always be directed towards lower values ($\Theta_m > 0$). The most general expression for the shift contains a weighted integral over an arbitrary distribution of the nonlinearity $\alpha(x)$.

$$\Omega_{res}(\varepsilon_m) \approx \Omega_{res}(0) \left[1 - \left(1 + \frac{4}{3\pi Q} \right) \frac{\varepsilon_m}{L} \int_0^L dx \alpha(x) \left| \sin^3 \left(m \frac{\pi}{L} x \right) \right| \right]$$

Nevertheless, in a first approximation the shift is always linear in the strain response. We can easily interpret the (sine)³ dependence on the position x_c of the damage in the above expression keeping in mind that modes will contribute to the nonlinearity to an amount which is proportional to their strain-field amplitude at the defect position. In the case of a hysteretic nonlinearity, the shift is essentially the result of a two-fold nonlinear interaction of mode m which affects the same mode m . The absolute value operation is the consequence of the non-uniqueness of the stress-strain relation. Further, we notice that the shift for a localized damage feature depends on the “effective” nonlinear strength parameter $\alpha w/L$.

In an analogous way we can also derive expressions for the generation of the odd harmonics in the above considered hysteretic system. For the third harmonic in the case of a localized damage we have found that

$$\varepsilon_{3m} = \frac{8Q}{5\pi} \frac{\alpha w}{L} \left| \sin\left(\frac{3m\pi}{L} x_c\right) \cdot \sin^2\left(\frac{m\pi}{L} x_c\right) \right| \varepsilon_m^2 = \Upsilon_m \varepsilon_m^2$$

The analytical results obtained for the one-dimensional case of resonance allow us to infer the location and the effective nonlinear strength of a single defect by simply considering the nonlinear signature on the lowest two resonance modes ($m=1$ and $m=2$). This yields the following theoretical reconstruction formulas for the position and the effective hysteretic strength:

$$\frac{x_c}{L} = \frac{1}{\pi} \text{Acos} \left[\frac{1}{2} \sqrt[3]{\frac{\Theta_2}{\Theta_1}} \right]; \quad \alpha \frac{w}{L} = \frac{\Theta_1}{\left[1 - \frac{1}{4} \left(\frac{\Theta_2}{\Theta_1} \right)^{2/3} \right]^{3/2} \left(1 + \frac{4}{3\pi Q} \right)}$$

which can be used as a first order identification of the defect location and its degree. If we use the strain dependence of the resonance frequency shift and of the third harmonic at the fundamental mode ($m=1$), we find that

$$\frac{x_c}{L} = \frac{1}{\pi} A \sin \left[\sqrt{\frac{3}{4} - \frac{5\pi \Upsilon_1 (1 + \frac{4}{3\pi Q})}{32 Q \Theta_1}} \right], \quad \alpha \frac{w}{L} = \frac{\Theta_1}{\left[\frac{3}{4} - \frac{5\pi \Upsilon_1 (1 + 4/(3\pi Q))}{32 Q \Theta_1} \right]^{3/2} \left(1 + \frac{4}{3\pi Q}\right)}$$

For the inversion in the case of non-localized defects it is necessary to use the more general equations and more sophisticated optimization algorithms.

POLITO investigated the multimode nonlinear resonance ultrasonic spectroscopy in a numerical manner. Computations have shown that the position of the defect significantly affects, at any fixed mode (e.g. the fundamental), the slope of the curve of the resonance frequency shift vs. amplitude. In Figure 1a.1 (left), the resonance frequency for different modes is analysed for fixed defect properties ($x_c = L/4$, $\alpha = \text{fixed}$, $w = L/20$). In the case considered, we observe a much larger shift for mode 2. The shift is different for the various modes, being much larger when the defect is located in a zone where the strain is greater, and the slope θ_n of the relative frequency shift as a function of the maximum strain response is function of the mode order n (see analytical expressions of KULeuven above). This result is in agreement with recent experimental observations.

To introduce a procedure for imaging of the defect location, we exploit some results reported in Deliverable D6 for nonlinear resonances. In particular, for a given specimen, we first calculate the slope θ_n for the first N_H modes. Then we introduce the sensitivity function

$$f(x) = \sum_n \theta_n \sin^2\left(\frac{n\pi x}{L}\right) \quad n=1,2,\dots, N_H \quad [1a.1]$$

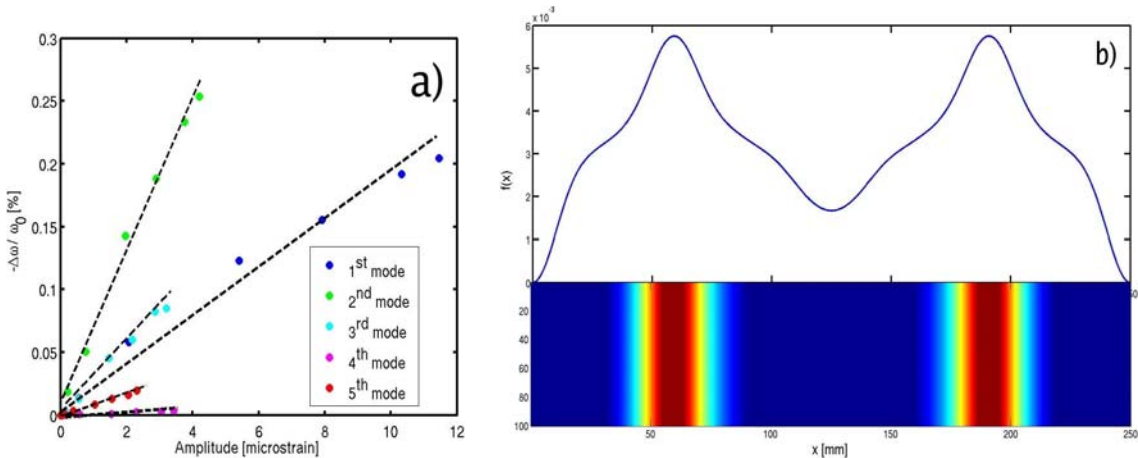


Figure 1a.1: (a) relative resonance frequency shift vs. strain amplitude for different input frequencies, sweeping around the different modes of resonance of the sample; (b) function defined in Eq. 1a.1. The peaks indicates the location of the defects.

where x is the position along the specimen.

The choice of the sensitivity function is linked to the strain energy fields of the different modes. For a 1D free-free bar, these modes are proportional to $\sin^2((m\pi/L)x)$. Moreover, from a mathematical point of view, the above proposed sensitivity function also makes

sense for globally distributed damage. Indeed, Windels and Van Den Abeele showed that for both classical and hysteretic nonlinearities, there is no mode dependency in the slope coefficients when the damage is uniformly distributed. Since

$$\lim_{m \rightarrow \infty} \frac{2}{M} \sum_{m=1}^M \sin^2\left(\frac{m\pi}{L}x\right) = \lim_{m \rightarrow \infty} \frac{1}{M} \sum_{m=1}^M \left[1 - \cos\left(2\frac{m\pi}{L}x\right) \right] = 1 \quad [1a.2]$$

we necessarily obtain a sensitivity function that is independent of the position. The constant value is an indication of the ‘global’ degree of nonlinearity.

In Figure 1a.1 (a), we report the function $f(x)$ obtained for a specimen of length $L=250$ mm with a defect centred in $L/4$, choosing $N_H=7$ modes in the summation. The procedure seems to be extremely efficient in the determination of the defect position, except for the fact that due to the symmetry of the modes with respect to the centre of the specimen a defect is also detected in $3L/4$. This symmetry can be broken only by changing the experimental configuration, e.g. by keeping one boundary of the specimen fixed.

It is worth noting that with an increasing number of harmonic frequencies the localization of the damage becomes more and more precise and the peak of the curve narrower. The procedure seems to work also with a larger number of defects (see Figure 1a.2, where we have introduced a defect at the centre ($L/2$) and at $L/4$).

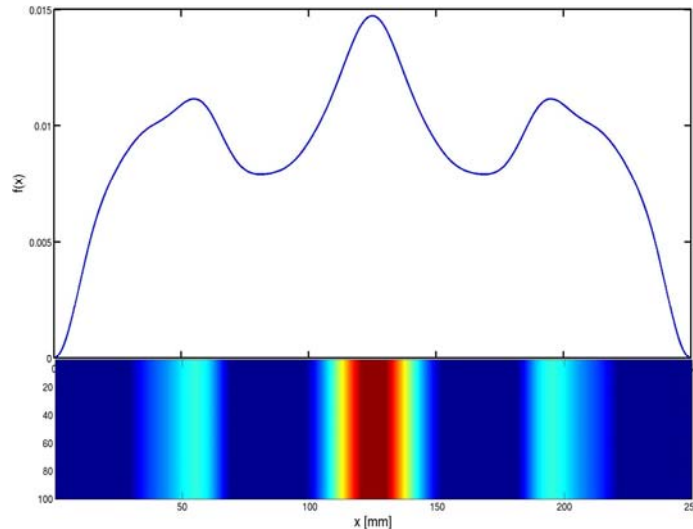


Figure 1a.2: Same as Fig. 1a.1, but with two defects, one in the centre of the sample and the other at $x=L/4$.

This localization method can be easily extended to more dimensions taking into account the nonlinear properties at various resonance modes, and weighing the contribution with the corresponding strain fields in 2D or 3D $\phi_{n,m}(x,y)$ or $\phi_{n,m,k}(x,y,z)$.

(1b) NEWS based Time Reversal technique

It is known that the sensitivity of NEWS methods to the detection of microscale features is far greater than what can be obtained with linear acoustical methods. However, most of the currently used experimental NEWS methods are based on a generalized interrogation of objects, for which the exact location of the defect domain structures is unknown (e.g. resonance, reverberation, etc.). At present most NEWS methods only specify whether the objects contain damage or not, and can be introduced in simple “fail-pass” quality control systems. In some cases this is sufficient, but there certainly exist additional demands for a “magical” system, which could promptly map the distribution of defects in a monitored structure.

Several types of acoustic and ultrasonic mapping systems for ‘linear’ scatterers already exist. Most of them are based on ray tracing or tomographic principles, or on the principle of time reversal invariance. The latter technique has been used for many years by seismologists in the petroleum exploration community (known as Time Reversed Migration) and has become a hot topic of innovative research in ultrasonic applications (mainly for fluids and soft solids, tissues) in the last 10 years primarily by the work of the group of Prof. M. Fink at the Laboratoire Ondes et Acoustique at the Université Paris 7. The basic premise of Time Reversed Migration (TRM), or simply Time Reversal (TR) as we will call it here, is the following: If the wavefield can be known as a function of time on some boundary surrounding a given region, then it can also be found at every point inside that region at previous times by using the wave equation with time running backwards. In other words, the result of a time-reversal process is that the waves recorded on the boundary are focused back in space and time on the acoustic sources, or on the scattering targets inside the region which were acting as sources. One of the benefits of TR is that it enables us to locate strong scatterers (voids and interfaces with high impedance contrast) which are hidden inside a region. In view of this, it is not a wonder that the interest in TR has recently grown considerably in connection with applications in shallow water oceanography, human body diagnostic and therapeutic treatment, land mine detection and applications to inhomogeneous material characterization for NDT purposes. An important advantage of TR for engineering materials is that it works extremely well in heterogeneous media (actually better than in homogeneous ones). Multiple scattering in transmission experiments or multiple reflections in waveguides, instead of being a hindrance, actually improve the focusing, to below the diffraction limit of about half of a wavelength. This reduces the number of receivers needed to obtain a good reversal quality.

Concerning NDT applications, however, researchers have encountered a serious limitation of the traditional TR technique in the fact that the scatterers have to be strong enough in order to be imaged, and that in fact only the strongest scatterer can be imaged. Successive TR iterations or the application of the so-called Décomposition de l’Opérateur de Retournement Temporel (DORT) method may overcome this feature to some extent and may enhance the detection by focusing selectively on weaker scatterers. In addition several signal processing techniques can be used to improve the efficiency of the TR process. Still, the sensitivity of classical TR to microdamage is quite low. The main reason for this is that the principle used in TR applications is based on *linear* time reversal, and relies on the wave propagation changes due to the *linear* scattering at

inhomogeneities in the material, i.e., reflections, refractions, mode conversions. Our experience in NEWS techniques have demonstrated that microdamage is first of all a process of *nonlinear* scattering giving rise to the creation of higher harmonics, rather than to “linear” scattering effects. So, from our point of view, the classical TR procedure should be modified in such a way that the main signal treatment is concentrated on the nonlinear components of the signals. For damage near the surface of an object, colleagues of the 'nonlinear elasticity of materials' group at Los Alamos National Laboratory recently suggested an enhancement of the TR procedure to isolate surface nonlinear scatterers by quantifying the local harmonic content and intermodulation distortion of high energy retrofocused signals upon scanning the surface of an object. For deeper defects, the alternative consists in selecting only the nonlinear/harmonic energy contained in the response signals and returning only this part back into the medium by the time reverse mirror. In the latter case, the time reversed signal will focus on the microdamaged area, which is the zone where the harmonics were created, while “linear scatterers” will not show up at all. This combination of TR and NEWS will enhance greatly the diagnostic capabilities of both TR and NEWS techniques at many scales.

Within WP2, the goal is thus to exploit the successful results of NEWS techniques for damage diagnostics in aeronautical applications, and to extend the methodology to defect localisation (imaging) using a combination of nonlinear wave diagnostic techniques and time reversal methods.

To do this we are working on the following NEWS based Time Reversal methodologies, which we intend to further test and verify, both numerically and experimentally, in the course of this project.

- 1) If a medium contains nonlinear scatterers, in the form of a microcracked zone for instance, the frequency spectrum of a wave travelling through such a zone will be enriched (because of a nonlinear dynamic response) by the harmonics of the fundamental frequencies which are locally present. These harmonics will accompany the “linear” response signal to the receivers. Instead of time reversing the complete received signal (which will refocus on the strong “linear scatterers” and on the source), we eliminate all linear scattering information by filtering the received signal and keeping only the information at the higher (harmonic) frequencies. This filtering can be done by applying analogue and/or digital high pass filters or by wavelet transformations and inversions. Sending back the filtered signals at all receivers, we will now focus only on the locations of the “nonlinear scatterers”, and this will allow us to identify with high sensitivity the microdamaged zones within a material.

Alternative and more efficient filtering techniques were also developed within this project (see Deliverable D6). Both approaches thus first filter the received signals before sending them back in the medium in reversed order. NEWS is being used as a pre-treatment for Time Reversal. This methodology is called NEWS-TR.

- 2) If the scatterers are located close to the surface (as is usually the case from impact damage), we can use TR to focus energy on the surface and by analysing the harmonic content or nonlinear signatures (e.g. the PC-PS addition) in the retrofocalized signal, we can determine the extent of the damage at the surface. In this

approach the received signals are sent back in reversed order to a specific location in the medium. NEWS analysis is being used as a post-treatment for Time Reversal. This methodology is called TR-NEWS.

Various signatures of nonlinearity have been measured with NEWS-TR and TR-NEWS: harmonic generation, intermodulation, pulse inversion, etc. Figure 1b.1 gives a summary of the different methodologies and approaches that can be applied.

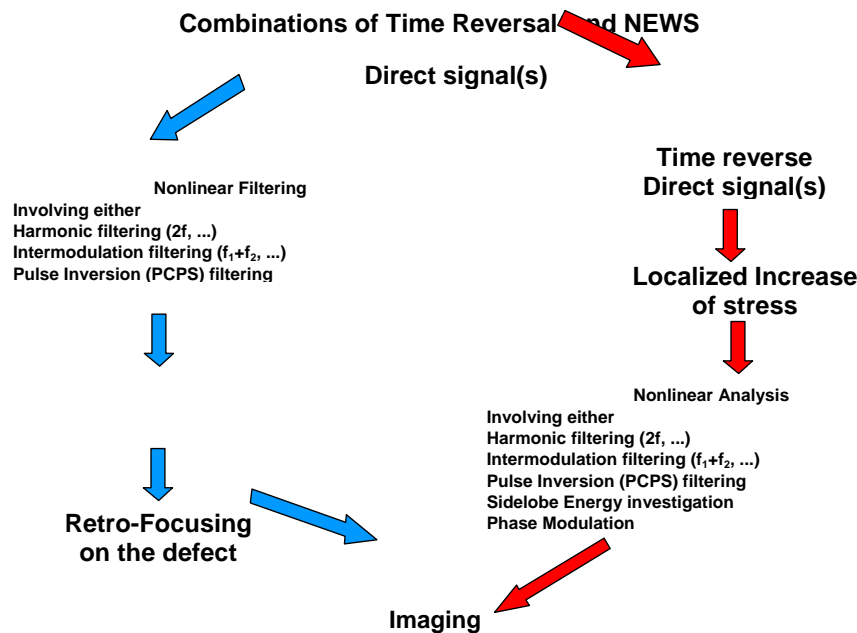


Figure 1b.1 : representation of the methods of defect detection using the combination of NEWS and TR.

It is important to know that time-reversal processes can be performed either numerically by computers using material models, or experimentally in the propagation medium itself, provided the simultaneous process of reversing and re-injecting the time signals can be realized experimentally. However, since the time reversal procedure (classical or NEWS based TR) actually only requires to analyse the linear back-propagation of the (linear or nonlinear) signals, we can perform the numerical TR calculations on linear material models, and use the method of superposition of individual signals for the experimental implementation.

The Time Reversal technique has been applied by GIP, KUL, POLITO and CU to simple 2D and 3D structures.

A common post-processing technique, here described for the two dimensional case, has been used by all partners in order to emphasize the defect location. Let us call $w(x,y;t)$ the function describing a certain field variable (vibration velocity, strain, stress, etc.) in any position (x,y) and at any time (t). We introduce the following function:

$$M(x, y) = \max_{t>0} [w(x, y; t)]_t \quad [1b.1]$$

which represents, in any position, the maximum value that the variable w assumes in time. The function M is expected to present maxima wherever focusing occurs and also maxima where the yet unfocused paths from the receivers interfere coherently towards the focusing point, hence identifying the ray paths. Here, we have chosen the field variable w to be the modulus of the local displacement vector field:

$$w(x, y; t) = \left\| \vec{u}(x, y, t) \right\| = \sqrt{u_x^2(x, y, t) + u_y^2(x, y, t)}.$$

Note again that the matrix M , which provides an image of the scatterer, as we will show, can be produced only using numerical simulations as data for the post-processing tools. It is currently not possible to acquire experimental signals at every point in a 3D object.

The following paragraphs summarise the results obtained by each partner.

(1b.1) POLITO

To simulate the propagation of ultrasonic waves in the specimen with nonclassical nonlinear inclusions, a two-dimensional (2D) and three dimensional (see Deliverable D9) LISA/Spring model has been used. In this particular case an aluminium plate of size 6 cm \times 12 cm has been considered. Two inclusions are present: one linear (a simple reduction of the Young's modulus) and another displaying nonlinear behaviour. The specimen is equipped with three extended transducers (size 10 mm \times 1 mm). Each of them is designed to force a stress into the specimen with Gaussian modulated profile (with centre frequency $\omega = 1.2$ MHz), placed as shown in Fig.1b.1.1.

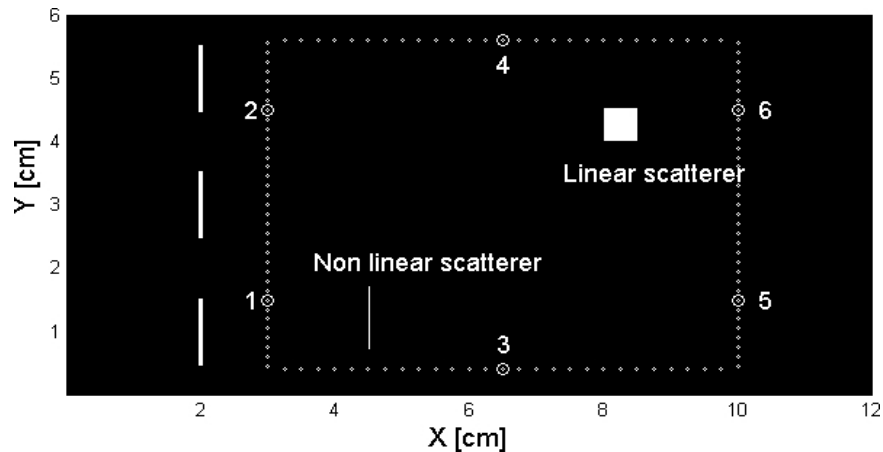


Figure 1b.1.1: Simulation sample with sources, receivers and defect positions.

To implement computational time reversal, the signals $u_j(t)$ recorded at each transducer j must be processed, time reversed and reinjected into a reference fictitious specimen with the same geometry and boundary conditions of the previous one, but without inhomogeneities and defects, at the same time from all transducers, now used as actuators. Due to the reciprocity in the wave equation, the phase delay between the reinjected signals $v_j(t)$ produces focusing on the position of the source of the original wave. Classical TR might be performed by using two different treatments of the received signals:

- **reversal processing**: it corresponds to the usual TR procedure. The injected signal is simply reversed in time. Therefore, in this standard procedure the portion of the signal due to scatterers is lost.
- **subtraction processing**: before time reversal, we subtract from the received signal the reference signal, i.e. the signal recorded at the same position in the absence of any scatterer. This processing analysis aims to eliminate the portion of the signal generated from the transducers only. Unfortunately, such an approach requires a baseline reference, which is not always available with the desired accuracy.

As a final step of the TR implementation, the processed signals are injected back into the specimen at the same time from all the transducers. Simulations of the propagation of the time-reversed field are performed using an homogeneous linear specimen (no scatterer), in order not to introduce any bias from an a priori knowledge of the defect location.

In Fig. 1b.1.2, we plot the map of the velocity field at the time corresponding to best focusing during the reversed propagation for the two processing procedures described: reversal and subtracting, from top to bottom. If one simply reverses the signal, the best focusing appears on the original source of the signal, i.e. on the transducers. Conversely, if one subtracts from the signal recorded at the receivers the signal produced in a homogeneous reference sample, the best retrofocalisation is on the linear scatterers, that have normally larger affects than nonlinear ones.

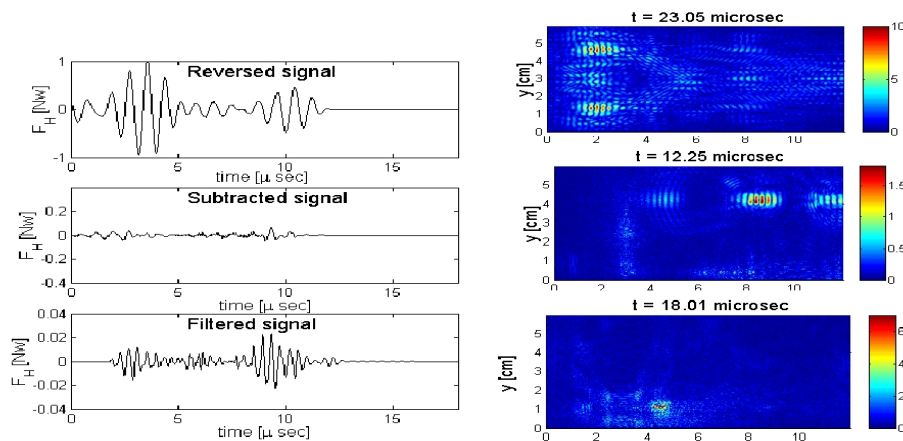


Figure 1b.1.2 : on the left column the injected signals in the TRA procedure. On the right map of the velocity field at the time corresponding to the best focusing.

Using the same sample, we performed a different treatment of the signal in order to analyse the effect of the nonlinear inclusion. Before inverting in time the signal we filter it with a high pass filter in order to eliminate the fundamental frequency of the signal and keep only higher order harmonics.

The processed signals are then injected back into the specimen at the same time from all the transducers. Simulations of the propagation of the time-reversed field are performed using a homogeneous linear specimen. In Fig. 1b.1.3, we plot the map of the velocity field at the time corresponding to best focusing during the reversed propagation.

Images of the wavefield at the time corresponding to best focusing yield a first indicator of the quality of the imaging procedure. In these plots, however, several pieces of information are lost. Much more better is to use the post-processing technique (Eq. 1b.1) described in the introduction and shown in Fig. 1b.1.4.

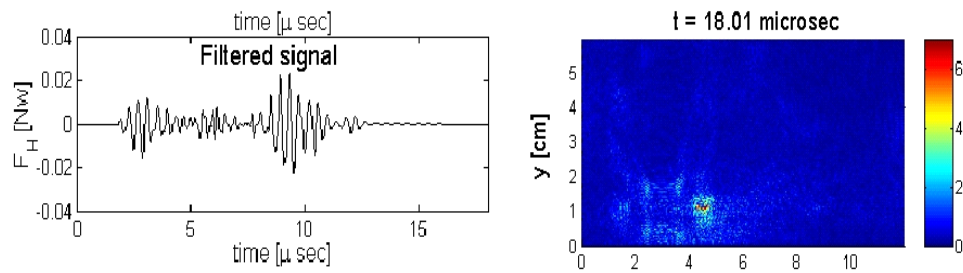


Figure 1b.1.3: On the left side the filtered and time reversed signal. On the right side the best retrofocalisation on the defect.

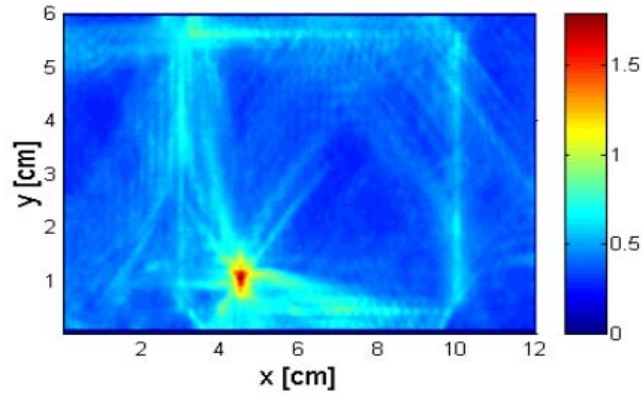


Figure 1b.1.4: Map of the maximum value in time of the displacement at each point of the sample.

(1b.2) KULeuven

KULeuven performed a numerical study of the Time Reversed Acoustic technique in 2D structures where source(s) and receiver(s) are both positioned on the surface of the sample. The simulations aim at visualizing a localized region of damage with a purely hysteretic equation of state represented by a uniform PM-space. A numerical NEWS-TR procedure corresponding to the proposed harmonic filtering NEWS-TR methodology was implemented. First, direct wave propagation experiments were simulated and the full time signals at certain receiver positions were stored. Second, the contribution from the third and higher harmonics of the fundamental frequencies, which originate from the damage region, was isolated by apodizing and Fourier-transforming the time signals, applying a filter in Fourier space and transforming the filtered spectrum back to the time domain. Finally, the filtered signals were time-reversed and reinjected back into a linear material model to check the retrofocalisation of the harmonics at the position of the defect. The results of these computations indicate that effective retrofocalisation strongly depends on the number of sources and receivers and on the relative position of sources and receivers with respect to the location of the defect.

Typical results are shown in Figure 1b.2.1. Here a steel sample with dimensions $20 \times 5 \text{ cm}^2$ and free boundaries is considered with a square region of damage (dimensions $1 \times 1 \text{ cm}^2$) in the centre of the sample located at $x = 10 \text{ cm}$, $y = 2.5 \text{ cm}$. The value of the hysteresis parameter is $\hat{\gamma} = 10^{-3}$. In the first simulation, a line source covering all points on the left side of the sample emits a short pulse with centre frequency 250 kHz and a particle velocity amplitude of 10^{-3} m/s , and all points on the right side act as receivers/sources in the NEWS-TR experiment. The total duration of the forward simulations is 100 μs , and 150 μs for the NEWS-TR simulations.

Figure 1b.2.1a shows a plot of the maximum mean stress at each point of the sample in the course of the NEWS-TR simulation. The mean stress time signal at the centre of the defect is shown in Figure 1b.2.1b. Both plots indicate a strong and unambiguous retrofocalisation on the defect region.

In Figures 1b.2.1c and 1b.2.1d, the same experiment is repeated, but the width of both the source and receiver regions is now restricted to 1 cm, centred at $y = 2.5 \text{ cm}$. The reduced energy input of the source and the loss of information at the receivers now leads to inefficient retrofocalisation at the defect. The last two panels, Figures 1b.2.1e and 1b.2.1f, show how the situation can be improved considerably by increasing the excitation amplitude at the source 25 times, so that the amplitude of harmonic generation increases 625 times. The retrofocalisation on the defect region is now obviously improved, although the time signal shows a more complicated structure and some energy in the NEWS-TR simulation is redirected back to the antipodal point of the source.

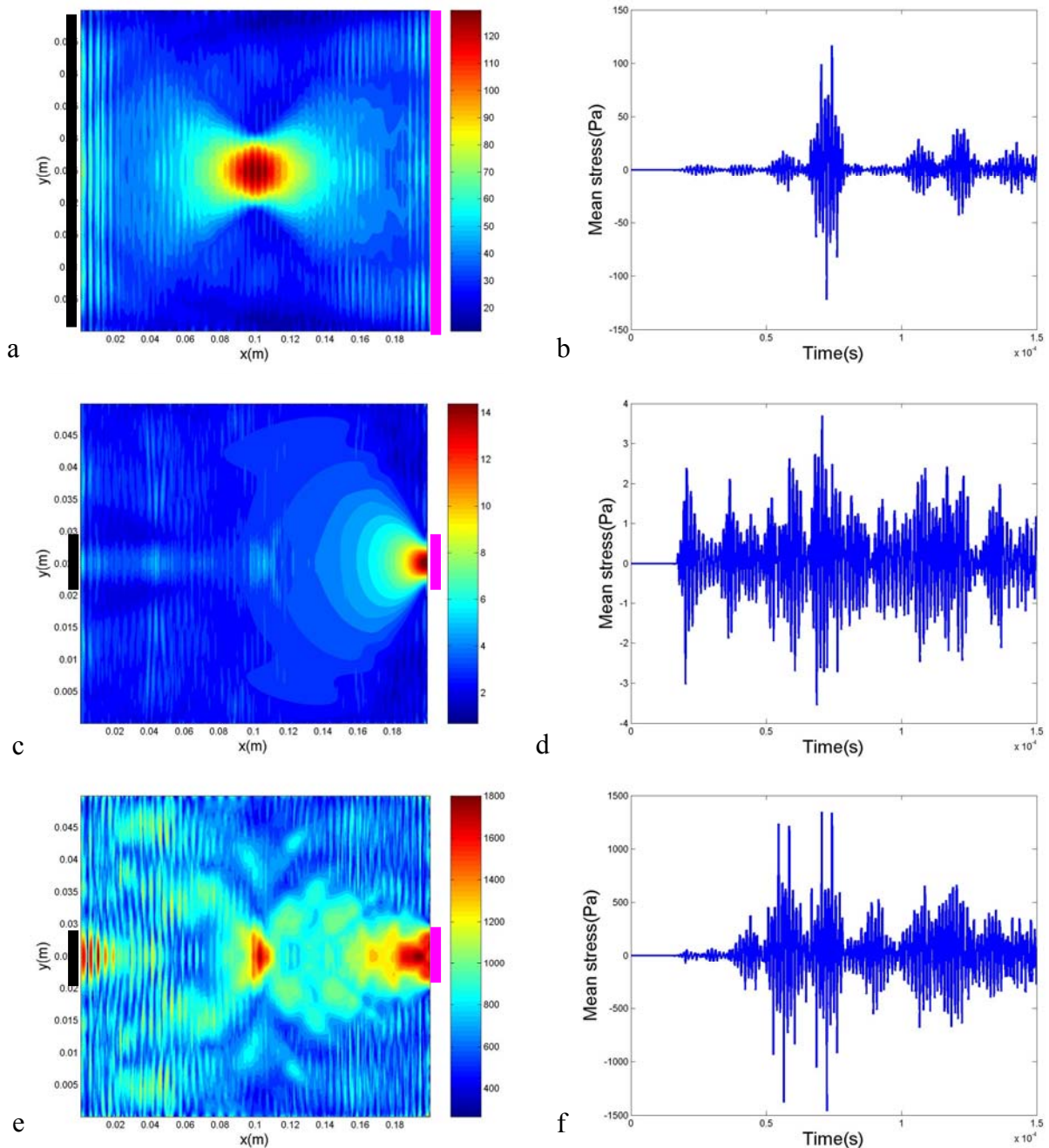


Figure 1b.2.1. Simulations of the NEWS-TR experiments using the harmonic filtering analysis approach in a 20cm x 5cm steel sample. A zone of localized damage is concentrated in the centre of the object. Left: maximum mean stress plots during the NEWS-TR simulations. Right: Maximum stress time history in the centre of the damage.

Top figures: source=5 cm on the left edge, excitation= 10^{-3} m/s, receivers=5 cm on the right edge.
 Middle figures: source=1 cm on the left edge (centred), excitation= 10^{-3} m/s, receivers=1 cm on the right edge (centred).
 Bottom figures: source=1 cm on the left edge (centred), excitation= $25 \cdot 10^{-3}$ m/s, receivers=1 cm on the right edge (centred).

Figure 1b.2.2 illustrates the importance of the source position with respect to the defect. The geometry and procedure is the same as before, but now the line source is located at the upper surface, extending over a width of 4 cm centred at $x=10$ cm, whereas the receivers remain in the same place and cover the full length of the right side. In this situation, where the source is sending most of its energy right towards the defect, we observe an efficient retrofocalisation at the defect region (Figs. 1b.2.2a and 1b.2.2b). On the other hand, if the centre of the source is displaced to $x=5$ cm, the defect is insufficiently activated and retrofocalisation is significantly inferior.

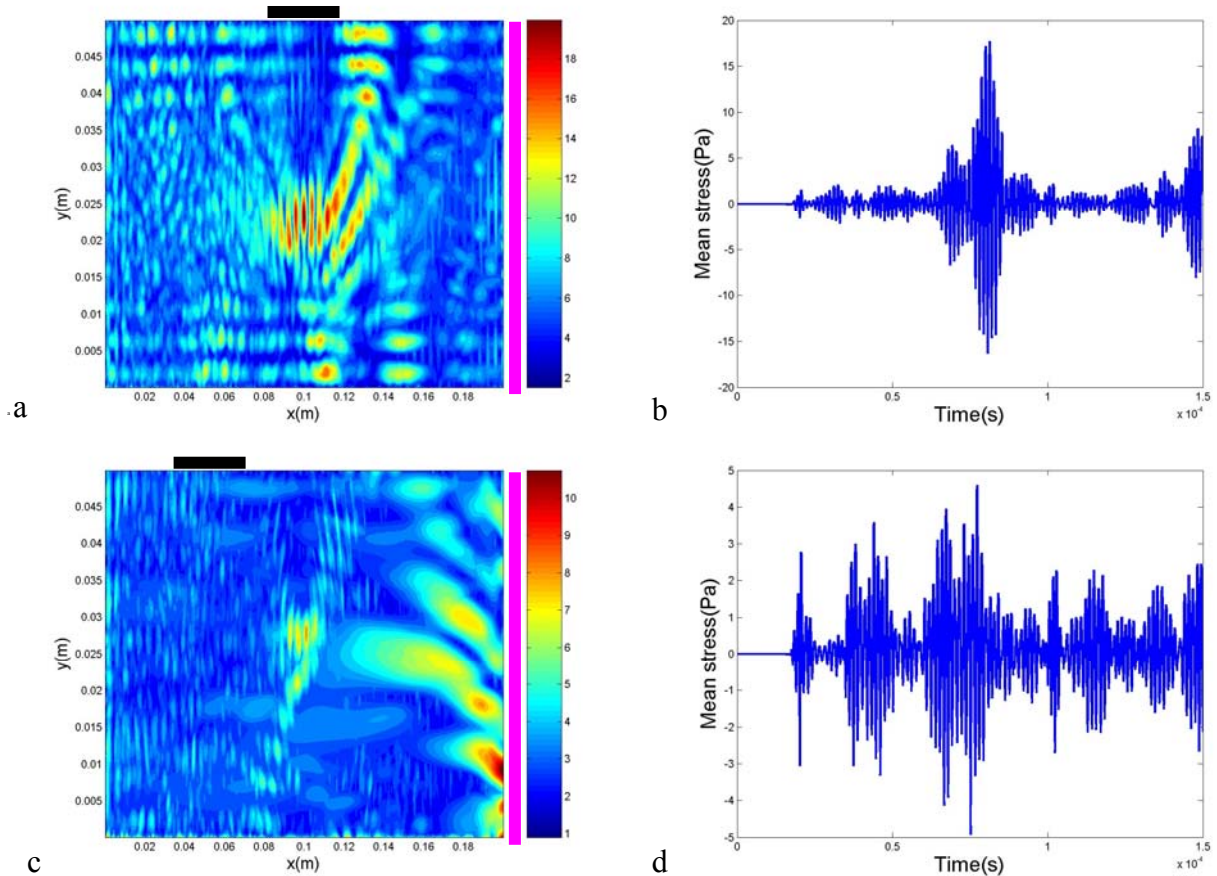


Figure 1b.2.2. Simulations of the NEWS-TR experiments using the harmonic filtering approach in a $20\text{cm} \times 5\text{cm}$ steel sample. A zone of localized damage is concentrated in the centre of the object.

Left: maximum mean stress plots during the NEWS-TR simulations.

Right: Maximum stress time history in the centre of the damage.

Top figures: source=4 cm on the top surface centred at $x=10\text{cm}$, excitation= 10^{-3} m/s, receivers=5 cm on the right.

Middle figures: source=4 cm on the top surface centred at $x=5\text{cm}$, excitation= 10^{-3} m/s, receivers=5 cm on the right.

KULeuven also performed several virtual experiments using the harmonic NEWS-TR methodology:

Simple geometry sample

Assume a steel sample of $20 \times 5 \text{ cm}^2$ with free boundaries and a region of microdamage (represented by hysteretic nonlinearity) at the centre. Further, suppose that a source is embedded within the sample and that the normal component of the velocity is recorded at all boundaries of the sample. Details of the configuration are illustrated in Fig. 1b.2.3a.

We filter the recorded signals using a harmonic filtering procedure, eliminating the fundamental component and retaining only the harmonic energy. The filtered signals are then inverted in time and reinjected in a linear material model.

The duration of the direct wave propagation simulation was $60 \mu\text{s}$. Fig 1b.2.3b shows the distribution of the magnitude of the velocity within the sample at $t=33 \mu\text{s}$ as an illustration of the retrofocalisation of the harmonics on the defect region. The corresponding time signals at the centre of the damage zone and the source are shown in Fig. 1b.2.3c (response of NEWS-TR). Finally, Fig. 1b.2.3d illustrates the time signals at the centre of the source and damage zones when a full time reversal is applied, showing retrofocalisation of the full time signals toward the source instead of the damage region this time.

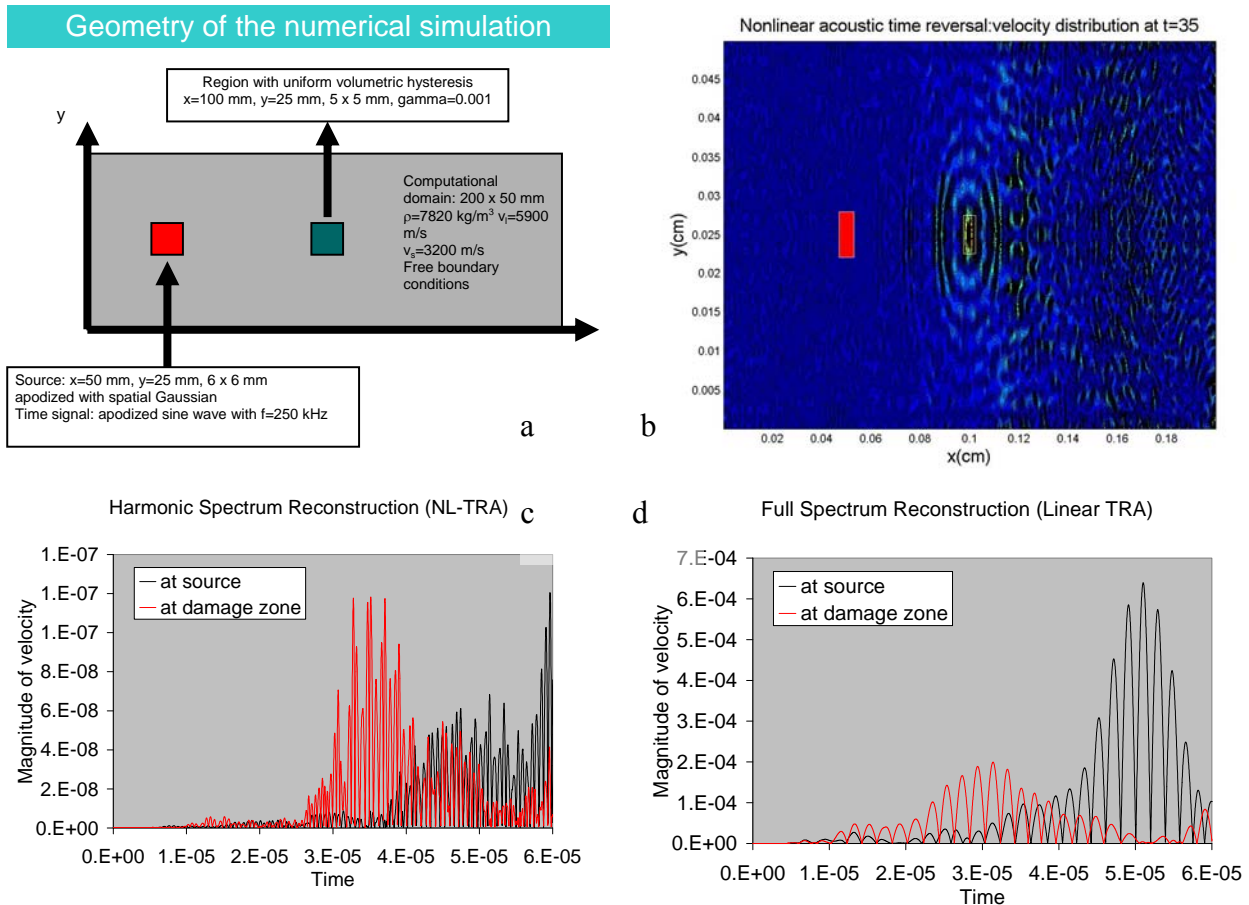


Figure 1b.2.3

Complex geometry sample

In addition to the previous simulation, a simulation was done on a slightly more complicated structure: an aluminium I bar.

The sample has an overall length of 200 mm in both the x and y directions. The structure consists of two pieces with dimensions 50 x 200 mm which are connected through a bar of size 100 x 50 mm. The values of the material parameters used in the simulations are given by $\rho = 1235 \text{ kg/m}^3$, $v_l = 2700 \text{ m/s}$ and $v_t = 1400 \text{ m/s}$, respectively. Free boundary conditions are applied at the borders of the structure. In the regions of the computational domain which are not part of the I-bar, we approximate a vacuum by dividing the Lamé constants by a factor 10^5 and the density by a factor 10^3 . We checked that this numerical procedure leads to almost complete wave reflection at the borders of the I-bar so that effective free boundary conditions are obtained. Our simulations do not include classical attenuation of any kind.

The sample is excited by an apodized explosive source which is located inside the bulk of the material. The emitted waveform is a short pulse at 250 kHz. The sample also contains a receiver that is situated in the bulk and with horizontal and vertical widths equal to 2 mm and 160 mm, respectively (see figure 1b.2.4).

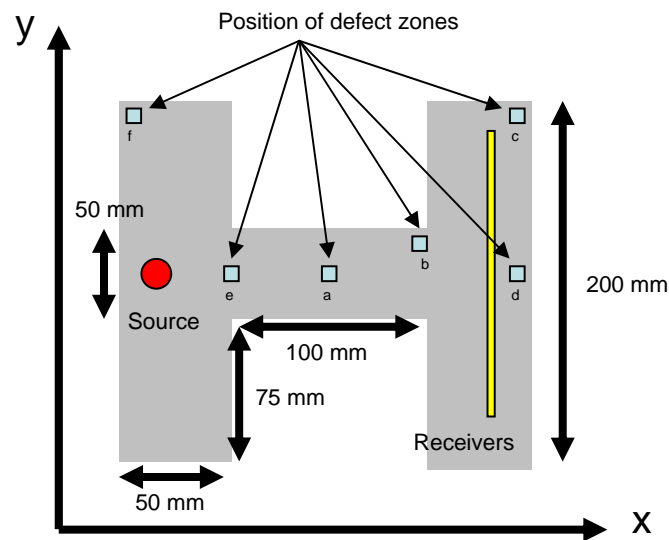


Figure 1b.2.4: Geometry of the I-bar for NEWS-TR simulations

The time-reversal process is implemented using the following procedure. First, the horizontal and vertical velocity components v_x and v_y are recorded at each zone within the receiver. The resulting time signals are numerically differentiated and multiplied by the density. In this way one obtains volume force densities f_x and f_y (in units of N/m^3). After filtering of the nonlinear content of the signals, these force densities are time-reversed and included as source terms in the right-hand sides of the equations of motion. The first part of this simulation, which follows the direct propagation of the waves in the sample, is continued over a time span of 400 μs (8000 time steps). The second part is a time-reversal simulation which lasts 600 μs .

We simulate NEWS-TR experiments by assuming the presence of a small defect zone with uniformly distributed microdamage over a square region of 10×10 mm. The microdamaged zone is modeled by imposing a hysteretic stress-strain relation with uniform (P_o, P_c) -distribution of hysterons and an individual hysteron strain contribution of $\gamma = 2.0 \cdot 10^{-17}$. The harmonic content of the signals is isolated by Fourier analysing the force volume densities, which have been stored previously as described above, and applying a high bandpass filter in Fourier space which retains the third and higher harmonics generated by the hysteresis in the damage zone. When this operation is completed, an inverse Fourier transform is applied, and the resulting force densities are time-reversed and reinjected back into the sample at the position of the receivers.

Figure 1b.2.5 illustrates the results of numerical experiments performed in the way described above. Again, the direct and time-reversed wave propagation simulations run over 400 and 600 μ s, respectively. Matrix plots of the maximum mean stress upon time reversal of the filtered signals are shown for 6 different locations of the centre of the damage zone. The positions of the microdamaged regions in the sample corresponding to the different plots in the figure are illustrated schematically in Figure 1b.2.4.

First of all, we clearly see that the NEWS-TR procedure is reasonably effective in identifying the region of the sample containing damage. The amplitude of the time-reversed harmonics depends on the relative position of the source and the damage zone. This is particularly evident in subfigure e, in which the defect is located close to the explosive source.

The NEWS-TR procedure also succeeds in locating defects in the upper right and left corners of the sample (subfigures c and f), although the retrofocused amplitude is considerably less in these cases. Furthermore, it is also important to note that the source itself emits some power at the frequencies where the high bandpass filter isolates the harmonics of the fundamental frequency. These waves separately focalize on the source as can be observed clearly in for instance subfigure c.

We refer to Deliverable D10 (Support and guidance for experimental procedures and methodology in terms of method selection, sensor and actuator placement and data acquisition) for a further analysis of the influence of receiver positions, time reversed information and signal length.

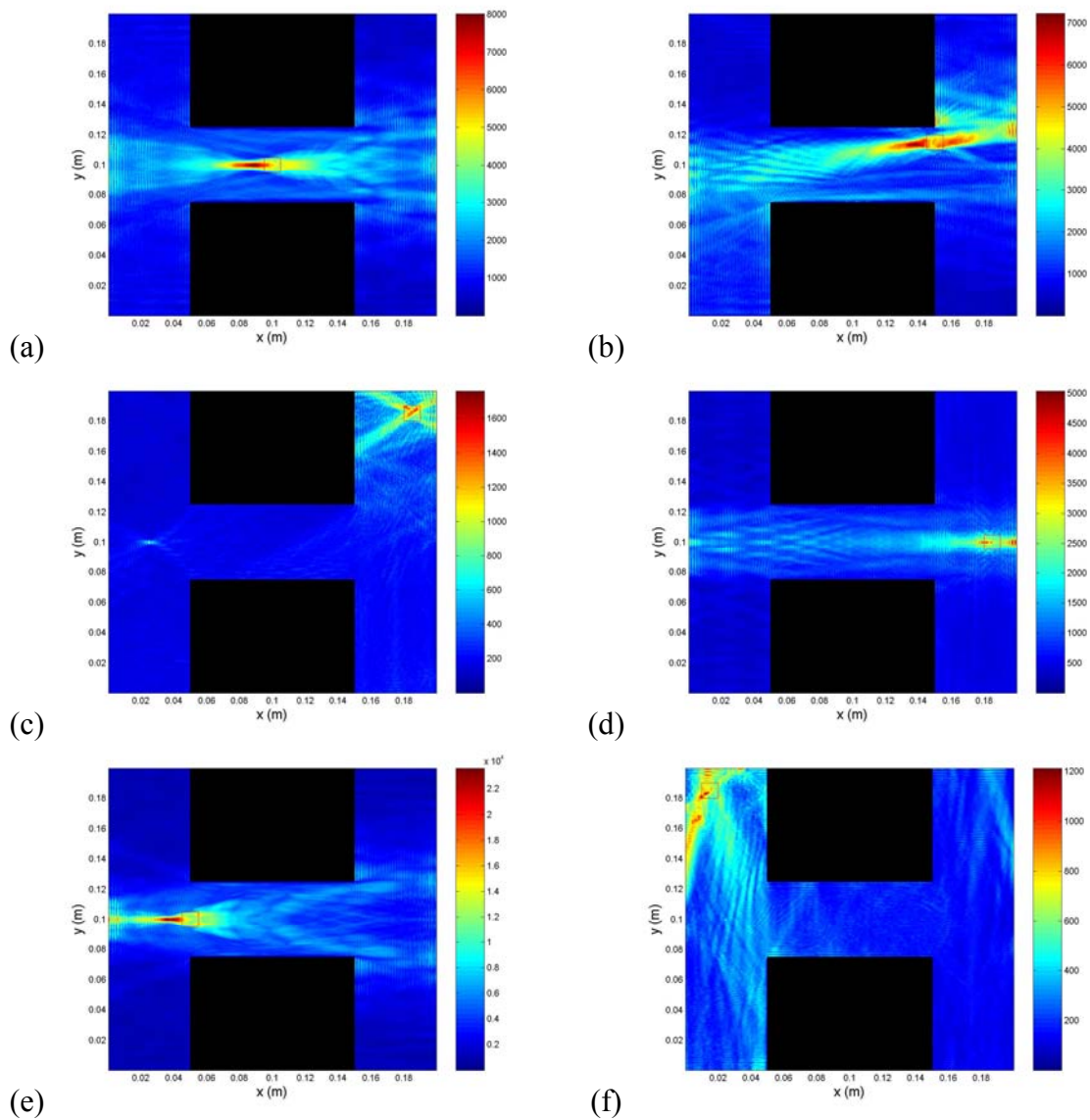


Figure 1b.2.5: Matrix plots of the maximum mean stress resulting from NEWS-TR simulations with six different positions of the damage zone. The position of the 10 x 10 mm damage zone is indicated by the open red rectangle in each plot. The timescale of the simulations is 400 μ s for the direct wave propagation simulations and 600 μ s for the time-reversed simulations after a high-bandpass filter has been applied to the received signals.

(1b.3) GIP-U:

In order to numerically test the NEWS-TR method, the simulation area (300mm×500mm) represented on Figure 1b.3.1 has been defined. The emitter is in the bulk (10mm×50mm) and the signal waveform is

$$f(t) = \pm p_0 \sin(2\pi f_c(t-t_0)) \cdot e^{-\frac{1}{2}\left(\frac{t-t_c}{w}\right)^2} \left(1 - e^{-\left(\frac{t}{s_w}\right)^2}\right) \cdot e^{-\frac{1}{2}\left(\frac{x-x_s}{w_x}\right)^2} \cdot e^{-\frac{1}{2}\left(\frac{z-z_s}{w_z}\right)^2}. \quad (14)$$

Receivers are in the bulk and are defined by 4 lines on 120 points (300mm), on 66 points (16,5mm) or on 20 points (50mm). Elementary hysteretic elements used to describe damage zone have triangular form (with an elastic behaviour before closing and linear after closing). Six different defect positions are defined to permit to show the influence of this position (Figure 1b.3.1).

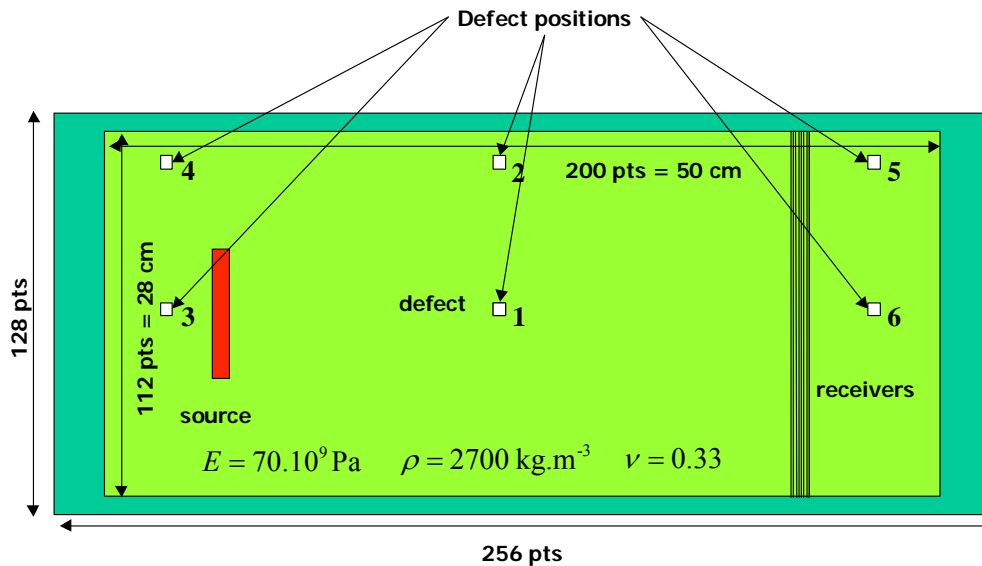


Figure 1b.3.1: Simulation area with material parameters and source, receiver and defect positions.

➤ Linear scattered and transducer reconstruction

To investigate the retrofocusing process in classical TRA (Figure 1b.3.2), simulations have been investigated where the signal received by the 4 lines is returned and remitted (by receivers). During the back propagation, maxima of amplitude are measured on each point of the bulk and the matrix obtained is plotted (Figure 1b.3.2).

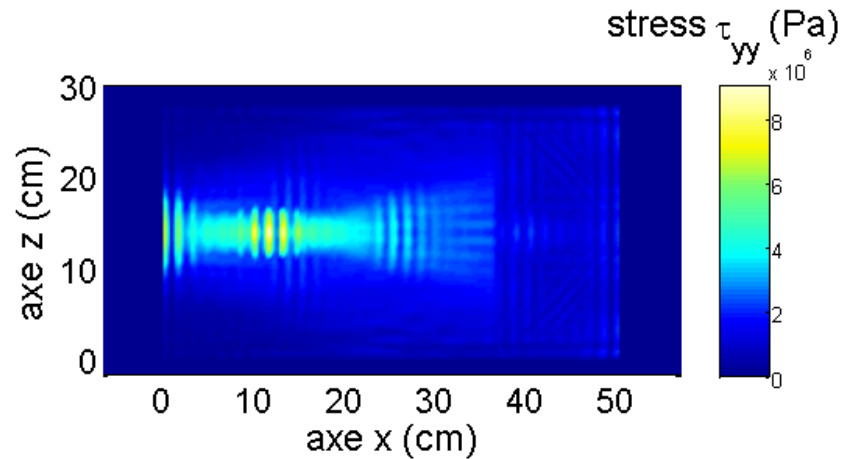


Figure 1b.3.2: : Matrix of the maxima of amplitude of stress component during the back propagation.

➤ NonLinear Time Reversal Acoustic

Generation of the harmonic frequency signal (called harmonic generation) and intermodulation were tested for nonlinear signatures. Two filtering methods were investigated for each signature, i.e. classical harmonic filtering and the pulse inversion method (also known as the phase-coded pulse sequence).

Filtering methods

Two filtering methods were investigated to return only the nonlinear parts (harmonics) of the received signal for NEWS-TR method i.e. harmonic filtering and pulse inversion.

a) Harmonic filtering

One option consists of selecting only the nonlinear/harmonic energy contained in the response signals and returning only this part back into the medium by the time reverse mirror. Hysteretic nonlinearity exhibiting high level of odd harmonics, the 3rd harmonic is extracted, in the next simulations, from the received signal using a 4th order Butterworth filter. The choice of this filter is justified by the perspective to use the NEWS-TR method in experiments.

b) Pulse inversion

An alternative filtering procedure is based on the fact that the phase inversion of a pulsed excitation signal (180° phase shift) will lead to the exact inverted phase response signal within a linear medium. This is not the case in a nonlinear (or microdamaged) material due to the generation of harmonics. Advantage of this information is taken by adding the responses from two phase-inverted pulses (positive and negative) and sending back the sum to the receivers. This operation is called ‘phase-coded pulse-sequence (PC-PS) filtering’ or ‘pulse inversion (PI)’. Only the relevant information on the local nonlinearities is reversed and sent back into the material.

Harmonic generation

Concerning harmonic generation effect, simulations have been done with defects in different positions and both methods of filtering have been used. For harmonic filtering method only the 3rd harmonic were returned on the bulk to retrofocus on the defect position and for the pulse inversion method, two opposite waves have been propagated from the emitter to receivers and the sum of the two received signals were returned. Four different results are presented for this generation (Figure 1b.3.3), two with a central defect (position 1) and two with defect at the edge (position 4).

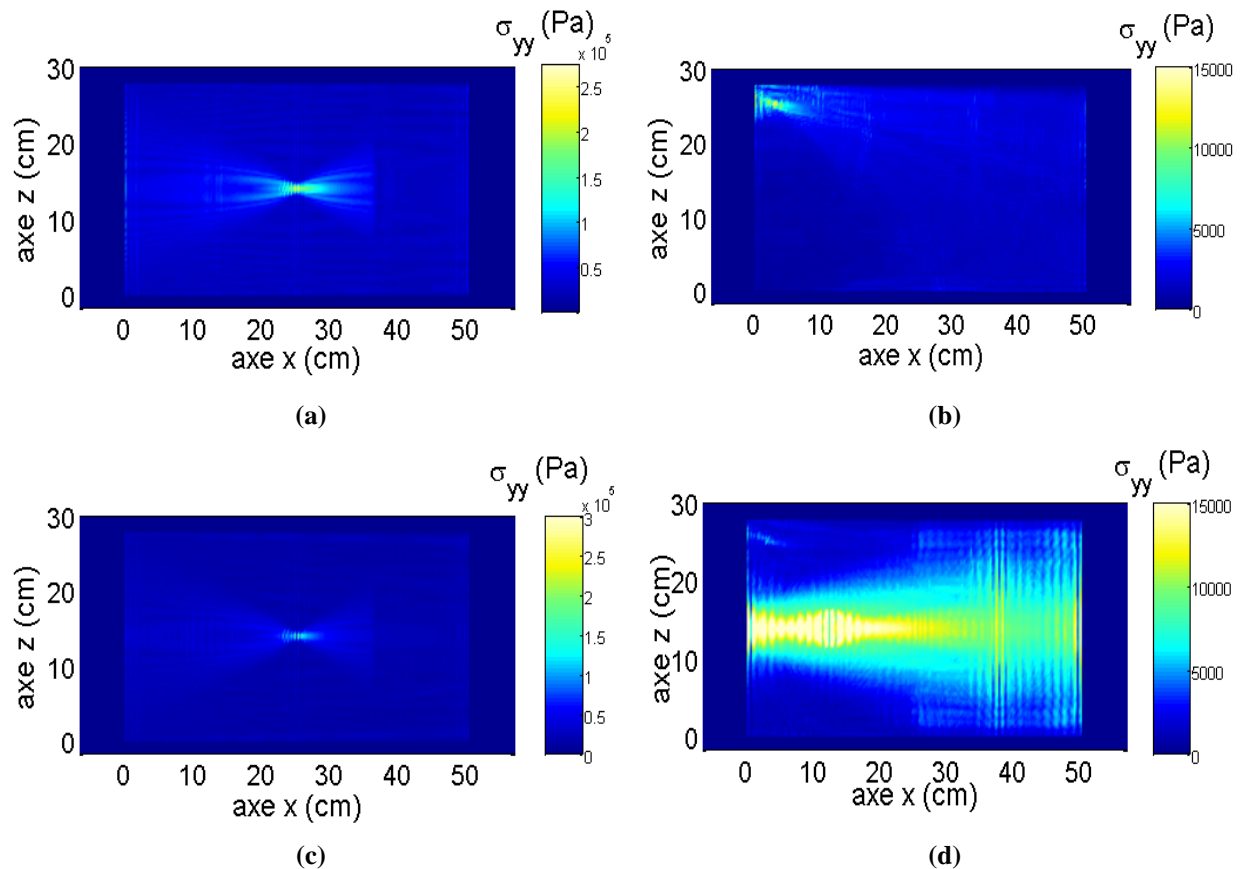


Figure 1b.3.3 : Matrix of the maximum of amplitude of stress components for the retrofocusing with pulse inversion method (a-b) and harmonic filtering method (c-d) for two different defect positions

Retrofocusing on the defect are different according this position and the method of filtering:

- If the defect is on the middle of the bulk (*i.e.* between emitter and receivers), retrofocusing spot is smaller with harmonic filtering method. This fact can be explained by the dependence of the spot size with the frequency; the higher the frequency is, the smaller the spot size is. Moreover, the smaller the source is, the less the focalisation spot size is large. However with harmonic filtering, 3rd harmonic is returned and with pulse inversion, 2nd harmonic is mainly returned.
- If the defect is at the edge of sample, retrofocusing is only on defect with pulse inversion. Energy of harmonics is smaller with the defect position 4 than the middle position, however with harmonic filtering, there is always small part of

fundamental frequency which is not filtered, whereas with pulse inversion this part is not present, and the ratio between this part and filtered harmonic (3rd for example) is higher in the case of edge position (less energy).

These remarks are well checked in Table 1b.3.1.

Table 1b.3.1: Comparison between the two methods of filtering for the 6 defect positions and for three source sizes.

	Ratio between amplitude maximum mean and amplitude maximum on bulk (with PI)	Ratio between amplitude maximum mean and amplitude maximum on bulk (with harmonic filtering)	Ratio between ratio with PI and ration with harmonic filtering
position 1			
300mm-source	6,44	9,31	0,69
165mm-source	5,67	9,66	0,59
50mm-source	3,93	4,34	0,90
position 2			
300mm-source	5,86	6,39	0,92
165mm-source	5,38	5,30	1,02
50mm-source	3,44	2,97	1,16
position 3			
300mm-source	7,08	6,88	1,03
165mm-source	6,24	6,15	1,01
50mm-source	3,36	3,28	1,02
position 4			
300mm-source	7,27	2,88	2,53
165mm-source	6,10	2,10	2,91
50mm-source	4,25	1,00	4,28
position 5			
300mm-source	7,35	6,38	1,15
165mm-source	6,00	5,68	1,06
50mm-source	4,12	4,13	1,00
position 6			
300mm-source	6,62	5,91	1,12
165mm-source	5,63	4,50	1,25
50mm-source	4,05	2,35	1,72

Intermodulation

Same simulation process than harmonic generation has been used for intermodulation. Two closed frequency waves ($f_1=200$ kHz and $f_2=300$ kHz) have been investigated. That permits to study the sum frequency ($f_+=f_1+f_2$) not close to f_1 or f_2 and so there is no influence of fundamental frequency.

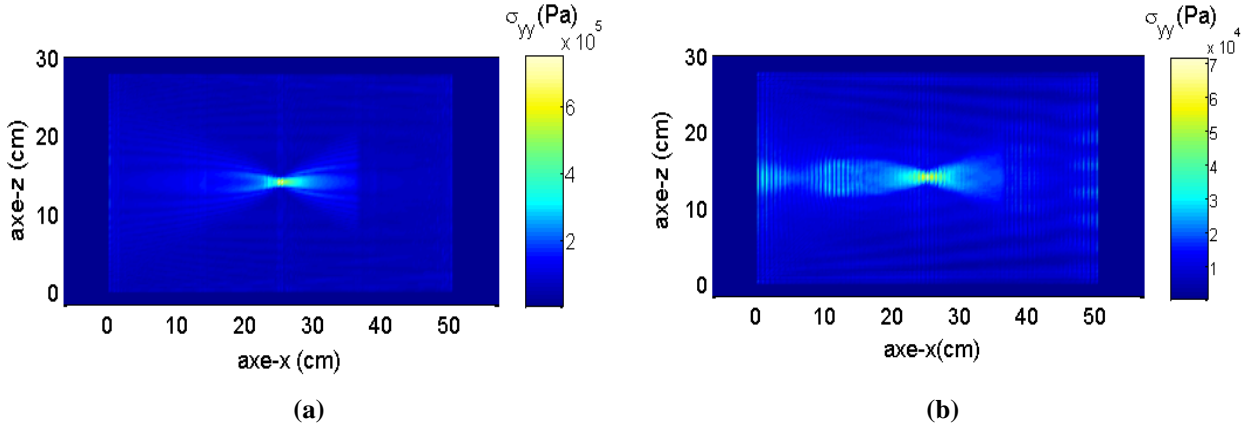


Figure 1b.3.4: Matrix of the maxima of amplitude during the back propagation at $f_+ = f_1 + f_2$ frequency (a) with pulse inversion method and (b) with harmonic filtering.

With pulse inversion filtering, retrofocusing on defect position is better than this with harmonic filtering. Figure 1b.3.5 compares the returned signal spectrum in the case of the harmonic generation (red line) and in the case of intermodulation (blue line). We can see that in the first case the returned signal has energy at harmonic frequencies (mainly 200 kHz, but also 600 kHz and 800 kHz). In the case of intermodulation (emission with f_1 and f_2), we have a great part of energy at $f_1 + f_2$ (500 kHz). In conclusion, not only all linear interactions are removed with PI filtering but also all the nonlinear interactions are returned.

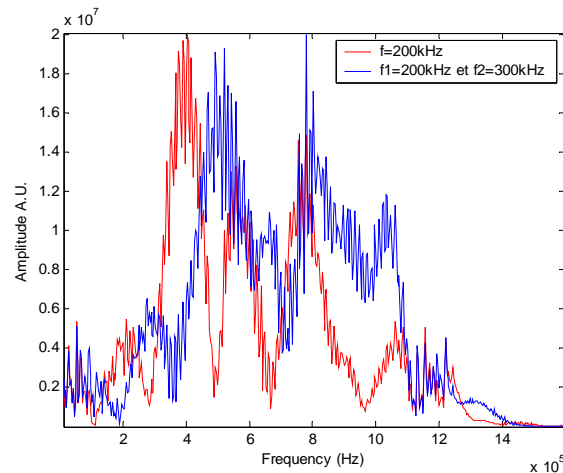


Figure 1b.3.5: Spectral representation of returned signal on harmonic generation (red line) and on intermodulation (blue line).

Two main differences between the method of filtering (harmonic filtering and pulse inversion) can be highlighted during this simulation study:

- Pulse inversion filtering is better for the defect detection near the edge of sample; all that relates to the linear propagation on bulk is freed with pulse inversion filtering contrary to that with harmonic filtering ;

- Harmonic filtering is more precise than pulse inversion when the defect is between emitter and receiver: the higher the frequency is (3rd harmonic), the more the spot size is small.

This conclusion allows us to tell that for the experiments, considering that emitter and receiver have finite size, it is better to move both emitter and receiver in order to place defect between them.

3D simulations (NEWS-TR & TR-NEWS method) in reverberant sample

➤ NEWS-TR method

To demonstrate the retrofocusing feasibility on defect position with returned nonlinear components and to study the quality of this retrofocusing, simulation geometry shown on Figure 1b.3.6 has been used. The material corresponds to an aluminium sample ($10 \times 2.5 \times 1.2 \text{ cm}^3$) with stress free boundaries and density $\rho = 8000 \text{ kg.m}^{-3}$, Young's modulus $E = 18,5 \cdot 10^9 \text{ Pa}$ and Poisson's ratio $\nu = 0.3$. A $5 \times 5 \times 1 \text{ mm}^3$ source is placed on the xy-plane (x and y are from 5 mm to 10 mm, $z = 1 \text{ mm}$), and emits a signal with frequency 250 kHz and amplitude 0.05 MPa. Receiver is composed of 1 line with a 25-mm length along y (receiver: $x = 60 \text{ mm}$, $z = 2 \text{ mm}$). The defects are composed of 5 points along one particular direction. Each 5 mm^3 -damaged zone presents a hysteretic nonlinear behavior and the rest of the sample is linear. Five different defect positions are defined to study their influence on the retrofocusing quality (Figure 1b.3.6): 3 defects along z (defect 1 centered in the material, defect 2 on a side, and defect 3 in a corner), defect 4 along x and defect 5 along y, both centered in the material.

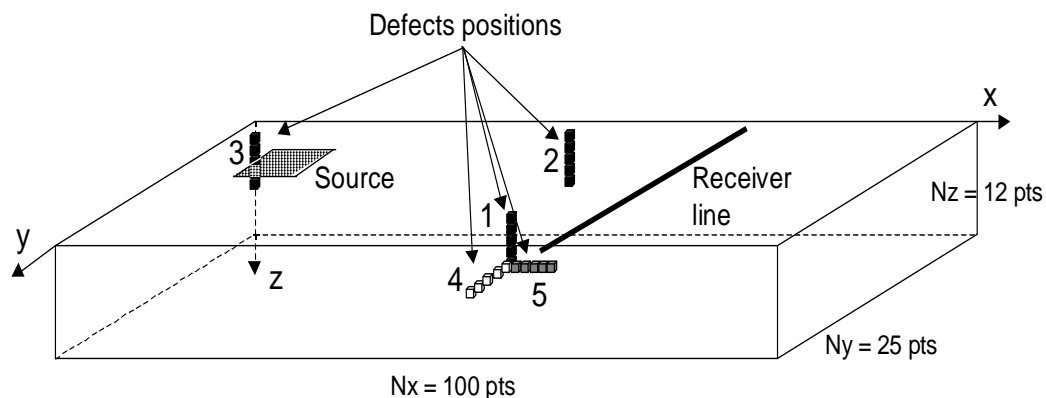


Figure 1b.3.6: 3D geometry of simulation domain with source, receiver and defect positions. Defects 1, 2 and 3 in black are along z, defect 4 in white along y and defect 5 in grey along x.

- Linear scattered and transducer reconstruction

A pulse emitted by the source is received by the receiver line, time reversed and emitted backward by the receiver. During the retropropagation, the maximum of amplitude, obtained for each point of the simulation grid, of 2 planes crossing the defect, is stored in 2 matrixes.

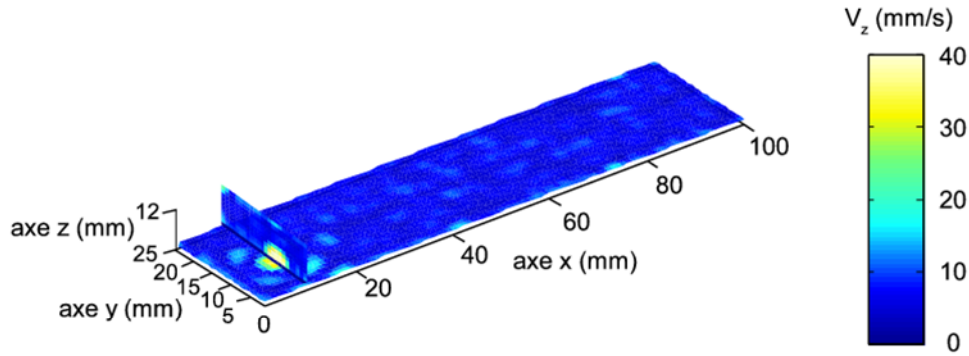


Figure 1b.3.7: Maximum amplitude of celerity component matrix obtained during linear retropropagation of the returned signal.

These matrices, presented on Figure 1b.3.7, shows following linear TR methodology, that the wave exactly retrofocuses on the source position. The focal spot size (around 5 mm) can be directly linked with the size and the shape of source and also with the emitted signal frequency. With linear TR process, defect which is on the center of the bulk (position 1) does not appear.

- NEWS-TR method

In order to localize damaged zone on the bulk, the direct signal, which propagated in the sample and was received by the receiver line, is filtered to keep only nonlinear components. Figure 1b.3.8 presents the results obtained in the case of the defect position 1 ($x = 50$ mm, $y = 12$ mm, z between 5 and 10 mm). It is obvious that the retrofocusing quality is better with the PI method that with harmonic filtering: higher amplitudes, more contrast and less noise on the sample sides. In the case of the defect 3 in the corner these observations are even more obvious.

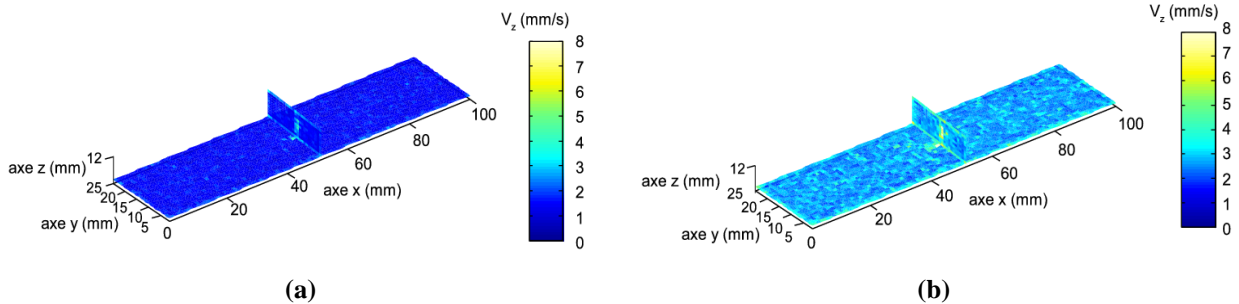


Figure 1b.3.8: V_z maximum amplitude matrix for the back propagation with defect position 1 with (a) PI method and (b) harmonic filtering.

Feasibility to realize defect imaging in a bulk using nonlinear signatures extracted from NEWS-TR has been demonstrated by means of 3D simulations. Future work consists in inserting experimental data in the model in order to verify, firstly, the retrofocusing on the source after time reversal, and, secondly, retrofocusing on a defect (on a side or inside the medium) after both time reversal and filtering.

➤ TR-NEWS method

The TR-NEWS method has been studied, where NEWS is a post-treatment after the TR process, which consists of locally increasing the stress field using properties of linear TR and subsequently applying nonlinear analysis. We verified the TR-NEWS methodology by a numerical investigation of the distribution of the harmonics in the point-by-point retrofocusing of energy for a 3D sample with a defect modeled by a zone with a nonlinear stress-strain behavior. The rest of the sample is supposed to be linear.

The defect position is: $x = 50$ mm, $y = 7$ mm and z between 1 and 5 mm. In the simulations, the material corresponds to an aluminum sample ($10 \times 2.5 \times 1.2$ cm³ corresponding to the size of ASCO sample, WorkPackage 1) with stress free boundaries and density $\rho=8000\text{kg}\cdot\text{m}^{-3}$, Young's modulus $E=18.5 \times 10^9$ Pa and Poisson's ratio $\nu = 0.3$. A fixed $5 \times 5 \times 1$ mm³ source is placed on the xy -plane, and emits a signal with frequency 250 kHz and amplitude 50 kPa.

As presented on Figure 1b.3.9, the pulsed signal, sent out by the source, is received by 9 different reception areas having the same size of the source. Following the TR-NEWS method, signals received by each reception area are time reversed and separately sent back from the original source without filtering. The newly received signal at the corresponding reception area, which is highly focused in time and space, is then filtered and the amplitude of the remaining signal at the focus in time is recorded. In our simulations, the signal filtering is realized using the pulse inversion (PI) technique. That means that two phase-inverted pulses (positive and negative) are separately emitted, returned, sent back by the source and their responses are summed at the reception area. The second harmonic (H2) amplitude is then analyzed for each retrofocusing area.

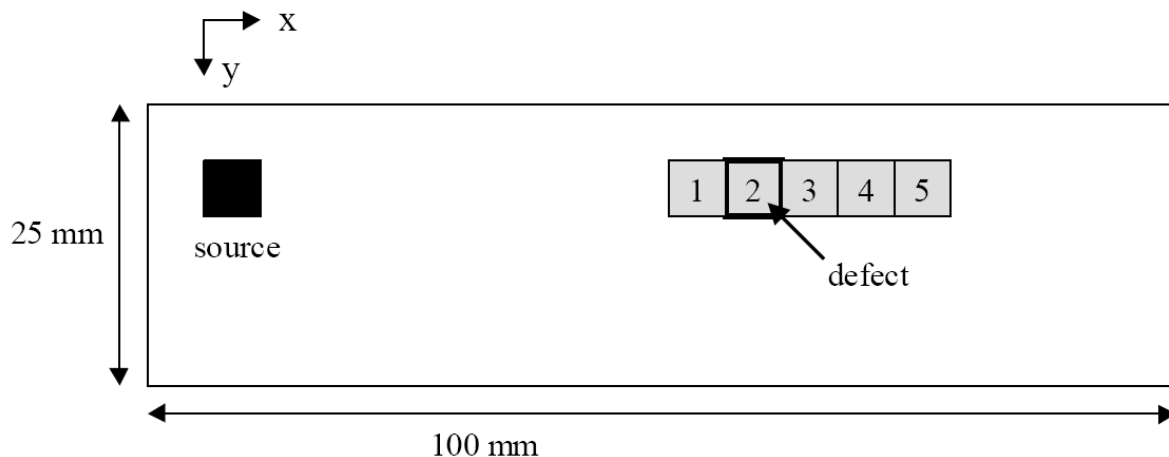


Figure 1b.3.9: Representation of a part of the simulation area (plane $x, y, z=1\text{mm}$). The gray squares represent the reception areas.

On Figure 1b.3.10 are represented the spectral representations of retrofocused signals after PI filtering for both the area 2, where is placed the defect, and the area 5. As expected, the H2 amplitude (500 kHz) is higher in the case of the area 2 (defect position).

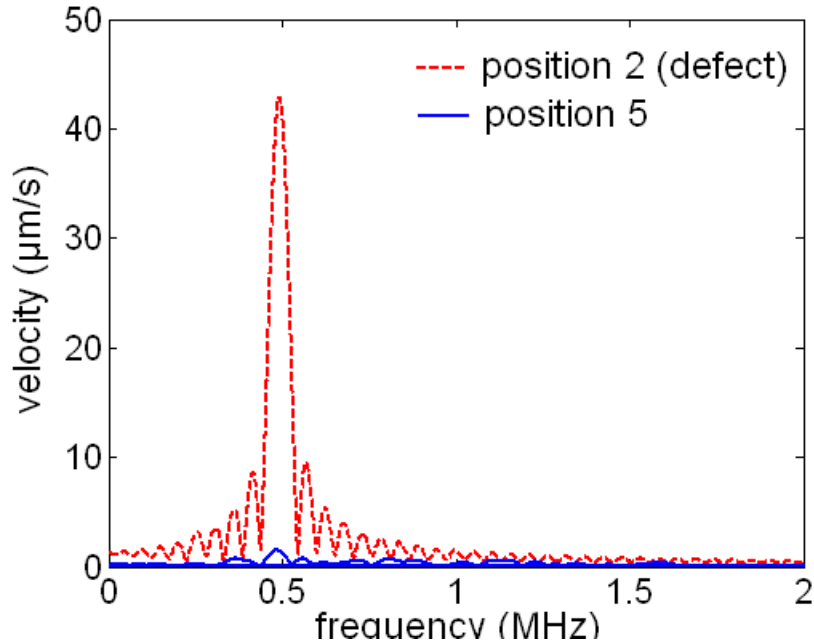


Figure 1b.3.10: Spectral representations of retrofocussed signals after PI filtering on the defect (dashed line) and around the defect (solid line).

Figure 1b.3.11 shows the evolution of the local harmonic content as a function of the retrofocusing area. With a relatively good precision, localization of the defect position is demonstrated (retrofocusing area 2).

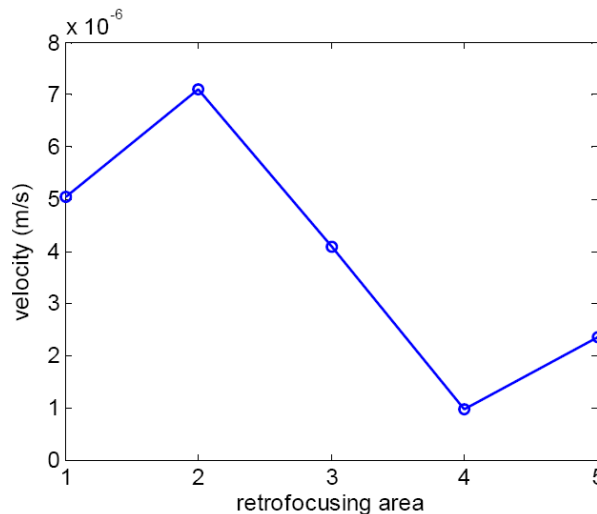


Figure 1b.3.11: Numerical calculation of the locally present harmonic energy H_2 in the retrofocussed TRA signals as function of the retrofocusing area, in horizontal direction.

- Chirp-coded excitation applied to NEWS-TR simulations

Time Reversal focusing improvement has been tested numerically using 2D chirp-coded excitation whose the form is defined on Eq.(15), instead of single-carrier short pulses (Figure 1b.3.12).

$$e(t, x, z) = -p_0 \sin(2\pi f(t)t) \cdot e^{-\frac{1}{2}\left(\frac{t}{2/f_c}\right)^2} \cdot \left(1 - e^{-\frac{1}{2}\left(\frac{t}{3/f_c}\right)^2}\right) \cdot e^{-\frac{1}{2}\left(\frac{z-2.5}{0.15}\right)^2} \cdot e^{-\frac{1}{2}\left(\frac{x-10.5}{0.75}\right)^2} \quad (15)$$

where $f(t) = \frac{f_{\max} - f_{\min}}{5000} * t - \frac{f_{\max} - 5001 * f_{\min}}{5000}$ with $f_{\max} = 1.7f_c$ and $f_{\min} = 0.8f_c$ and $f_c = 200$ kHz.

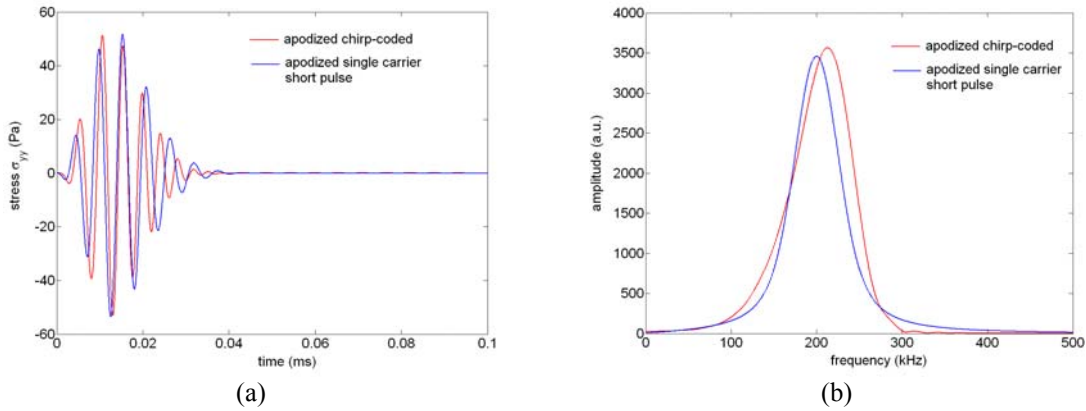


Figure 1b.3.12: (a) Temporal and (b) spectral representations of apodized chirp-coded signal (red) and apodized single carrier short pulse (blue).

The advantage of such optimization of excitation also used in medical ultrasound is its ability to transmit more energy per time without increasing the peak intensity.

The chirp-coded NEWS-TR consist in sending an apodized chirp excitation of 200 kHz central frequency, apply the correlation function between response of the transmitted signal on the medium and the excitation signal and use the result as an excitation instead of the impulse response.

The obtained 2D mapping of the stress component maximum of the re-emitted time reversed signal clearly shows the retrofocusing, in this simulated linear case, of the wave at the position of the initial source (Figure 1b.3.13). A similar result has been obtained with classical time reversal method, but with lower obtained maximum amplitude.

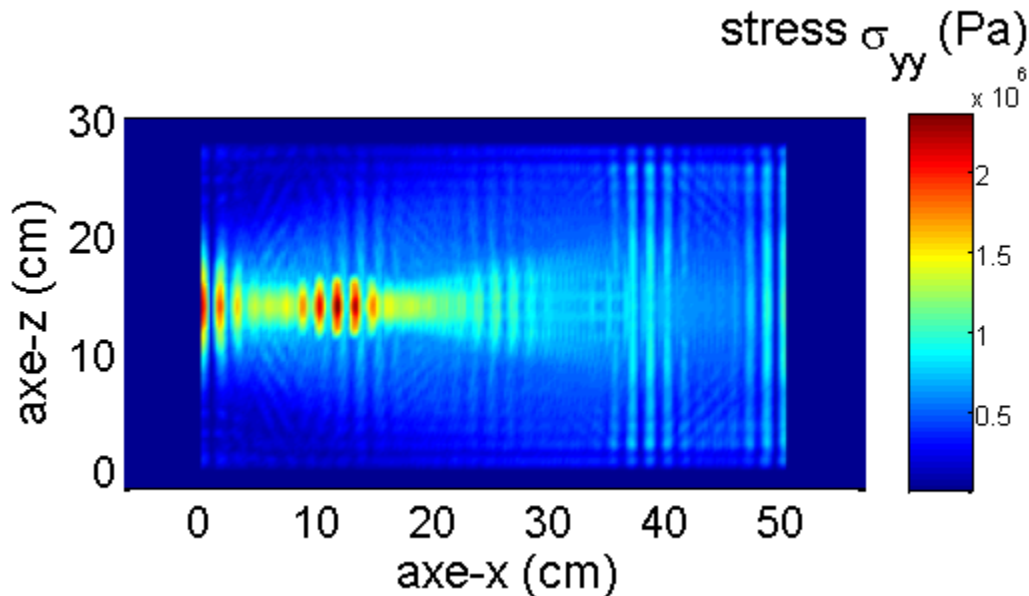


Figure 1b.3.13 : Validation of chirp-coded TR in 2D with a mapping of the stress maximum component. The retrofocusing is present at the position of the initial source ($x=12$, $z=15$).

The aim of this study is to show the applicability of chirp-coded excitation on the time reverse and nonlinear analysis process in order to increase the stress on the retrofocused area with the TR-NEWS procedure or to increase the amplitude of the propagated signal to have more nonlinear components with the NEWS-TR process.

Conclusion

The approach developed for this purpose was based on a 3D pseudospectral time domain algorithm. The elastic coefficient tensor was modified using the Kelvin notation, and hysteretic nonlinear behavior using the Preisach–Mayergoyz space model was introduced in the damaged area. Simulations performed on a metallic sample showed the feasibility and value of the NEWS-TR and TR-NEWS methodology for microdamage imaging. Chirp-coded NEWS-TR has been introduced as a new tool for performing retrofocusing on the damaged region. The 3D PSTD simulator confirms the fact that NEWS-TR and TR-NEWS methods are efficient tools for ultrasonic imaging of the nonlinearity of real complex samples.

(1b.4) Cranfield University

A new non-linear time reversal technique was developed for the detection and localization of stress corrosion cracking (SCC) damage in a friction stir-welded aluminium plate-like structure. A stir welded plate composed by two aluminium alloy plates (AA7075–T7351 and AA6056), 0.35 m long, 0.4 m wide and 5 mm thick, joined by 20 mm of weld, was object of investigation. SCC area was located at the welding interface (20 mm long and 8 mm wide). The corroded area was placed in the heat affected zone and modelled using a multi-scale material constitutive model (Preisach-Mayergoyz space) with uniform HMEU distribution $\mu(P_c, P_o) = 1$ between ± 5 MPa and $\mu(P_c, P_o) = 0$ everywhere else, for a maximum strain $\alpha = 0.001$.

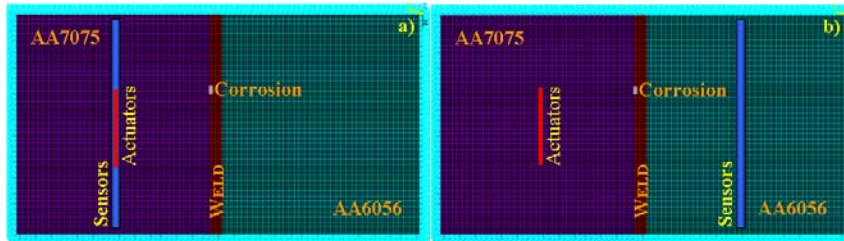


Figure 1b.4.1 – Actuator-sensor configurations.

A new non-linear damage detection imaging technique based on time-reversal acoustics was developed. Compared to the traditional TRA, the newly developed time-reversal method takes into account the non classical nonlinear material behaviour introduced by the cracked area. In particular, the presence of damage introduces in the dynamic structure response high order harmonics of the excitation pulse central frequency. The method consists in re-emitting in the structure selected time signals filtered with a pass band frequency filter centred at the third harmonic of the excitation pulse central frequency to have an ‘image’ of the faulted zone (Fig. 1b.4.2b). The 3rd harmonic was selected because of its larger energy content. Studies were conducted to select the optimum time window signal to reverse and to re-emit in the structures.

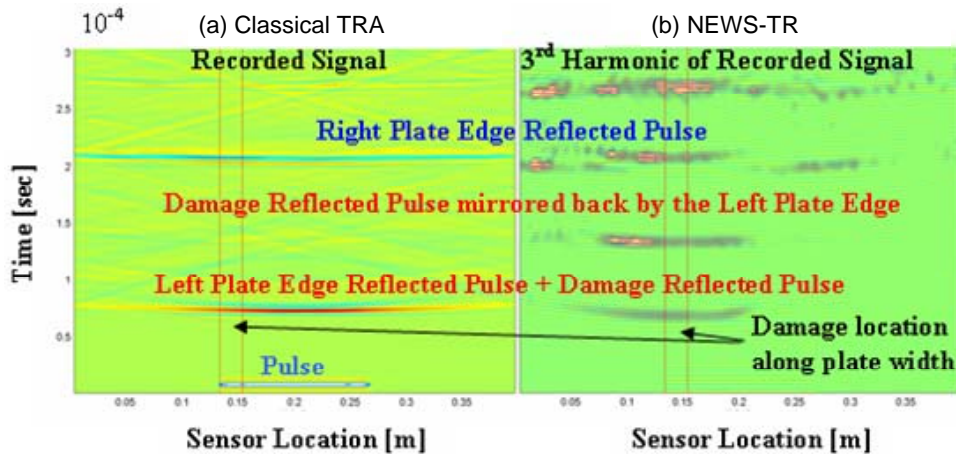


Figure 1b.4.2: Time window selection to reverse: a) classical time reversal acoustics; b) NEWS-TR.

The methodology was compared with traditional time-reversal acoustics (TRA) showing significant improvements. In particular, using the classical TRA (Figure 1b.4.3a) is re-emitted in the structure not only the damage, but also, the pulse on the actuator array location (Figure 1b.4.3a) is refocused, hiding almost the damaged refocused wave. On the contrary, by reversing only the 3rd harmonic of the selected RTW (Figure 1b.4.3a), only the damage is refocused and, therefore, a clear damage localisation was obtained.

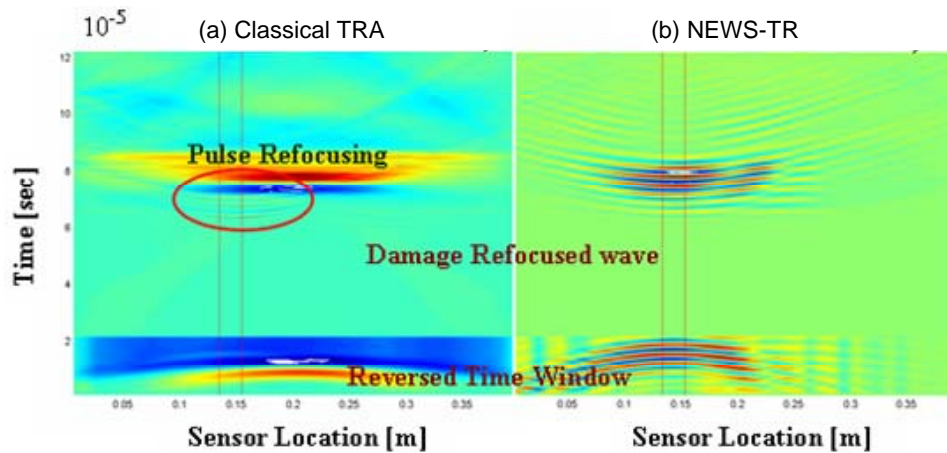


Figure 1b.4.3: Time-reversed signals for first configuration: (a) classical time reversal acoustics; (b) NEWS-TR.

The current results compared to the traditional TRA, shows that the new developed method was able to localize in a clear manner the faulted zone showing its robustness to detect and locate non-linear sources in presence of different materials.

D7.2. Investigation of the influence of sample geometry on the phases in nonlinear transmission experiments

The role of IZFP in WP2 is to reinforce the link with WP1, i.e. the support from an experimental and a practical point of view in order to ensure that the developments of numerical models and virtual experiments carried out in WP2 are guided by the actual experiments and measurements as well as the samples and components of real use in WP1. Within these objectives the partners POLITO and IZFP collaborated on 1D numerical modelling of nonlinear ultrasonic transmission experiments through thin bonded interfaces using LISA (POLITO), so far assuming no hysteresis in the interface vibrations.

Due to its symmetry in the direction normal to the wave propagation, the geometry of the experiment suggests the application of a 1D model for its numerical simulation. The 1D approach is applicable if we focus on the interstice deformation in an area at the centre of the specimen, whose transversal section is much smaller than the specimen length. Since we simulate linear elastic wave propagation except for a very localized nonlinearity (the interstice) we use the Local Interaction Simulation Approach (LISA). Its local character makes it particularly suitable for our experiment. We only have to replace the linear relation between stress and strain at the bonding by a nonlinear one. The LISA code is similar to the formalism of Finite Difference Equations (FDE). The specimen is divided into a number of equally sized homogeneous cells (of length δ and cross section α), whose masses are concentrated in a node, labelled with an index j . The bonding is located at $j = i$ (see Figure 2.1). The elastic behaviour of the material is described by springs connecting neighbouring nodes. Further details can be found in the corresponding references (see footnote).

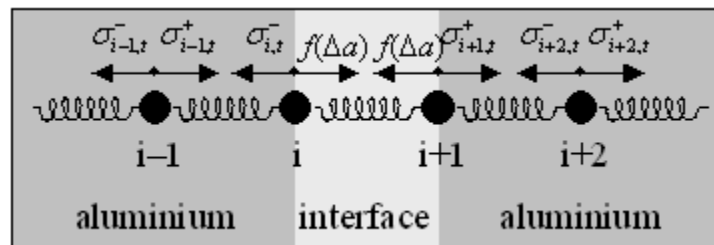


Figure 2.1. Discretisation of the specimen used for the LISA simulations.

Calibrated measurements have been carried out for a sample consisting of two aluminium plates of 4 mm thickness bound together by an epoxy layer of less than 0.03 mm thickness. The calibration procedure transforms the measured data from the receiver and the input transducer into the strain amplitudes and the phases of the fundamental and higher harmonics of the incoming and transmitted waves (see corresponding references in the footnote). Waves reflected from the borders of the aluminium slabs are eliminated. Therefore, in our LISA simulations we assume infinite aluminium slabs at both sides of the bonding. This is realized using a Perfectly Matching Layer (PML) of absorbing boundaries at both ends of the specimen. We choose the discretisation step δ equal to the static equilibrium width of the bonding a_s (approximately 0.03 mm). A monochromatic compressional wave with a frequency of 2.25 MHz is injected at the left end of the

specimen. Its wavelength in aluminium is about 100 times the discretisation step, ensuring sufficiently smooth description of the wave and that the effects due to finite propagation time of the wave through the interstice are negligible.

The numerical results are compared to experiments on nonlinear transmission of compressional ultrasonic waves perpendicularly incident onto the interface carried out at IZFP². Fig. 2.2 shows the numerical results as well as the experimental data of the first, second, and third harmonic as function of the input strain. Both simulations yield a very good agreement up to the threshold when hysteresis sets in. For larger excitation amplitudes the 2nd and 3rd harmonics show large discrepancies, suggesting that the aforementioned assumptions are no longer valid. Nonclassical effects, such as hysteresis of the higher harmonics, which are not included in the model, are responsible for these differences. Since these effects generally occur in the presence of defects in the bonding, the discrepancies may give a measure of the bonding quality. The agreement between theoretical and experimental results up to the nonclassicality threshold is a good indicator of the quality of the calibration procedure and shows that the measured nonlinearity actually stems from the adhesive interface. In fact, simulations performed from uncalibrated measurements (data not shown for brevity) yield a much poorer agreement with the experimental data.

For larger excitation amplitudes, when the ultrasonic stress amplitude in the interface approaches the bond strength, hysteresis in the interface vibration is no longer a small effect and causes phase shifts in the transmitted waves which might differ in dependence on the order of the harmonics. The phases contain important information especially if not only the amplitudes of the transmitted waves and the distortion factor as an overall measure of the nonlinearity is to be considered but a reconstruction of the interaction forces in the interface is aimed for³. This is demonstrated by the spectral analysis of a PM space unit, which is a special model describing some features of interaction forces, and

² P.P. Delsanto, S. Hirsekorn, V. Agostini, R. Loparco, A. Koka, "modelling the propagation of ultrasonic waves in the interface region between two bonded elements", *Ultrasonics* 40 (2002) 605-610.

P.P. Delsanto, C. Camagna, M. Hirsekorn, S. Hirsekorn, "Nonlinear Effects in the Propagation of Ultrasonic Waves through Thin Interfaces", 2nd Workshop "NDT in Progress", Prague, Czech Republic, Oct. 6-8, 2003, ISBN 80-214-2475-3 (2003) 69-74.

S. Hirsekorn, M. Hirsekorn and P.P. Delsanto, "Nonlinear Ultrasonic Transmission Through Thin Bonded Interface: Theoretical Background and Numerical Simulations", in "The universality of nonclassical nonlinearity, with applications to NDE and Ultrasonics", Ed. P.P. Delsanto, Springer, New York, 2005 (in print).

³ S. Hirsekorn, A. Koka, W. Arnold, "Theoretical and Experimental Investigations of Interaction Forces in Thin Bonded Interfaces by Nonlinear Ultrasonic Transmission", 2nd Workshop "NDT in Progress", Prague, Czech Republic, Oct. 6-8, 2003, ISBN 80-214-2475-3 (2003) 99-106.

S. Hirsekorn, P.P. Delsanto, "On the universality of nonclassical nonlinear phenomena and their classification", *Appl. Phys. Lett.* Vol. 84, Issue 8 (2004) 1413-1415.

P.P. Delsanto, S. Hirsekorn, "A Unified Treatment of Nonclassical Nonlinear Effects in the Propagation of Ultrasound in Heterogeneous Media", *Ultrasonics* 42 (2004) 1005-1010.

S. Hirsekorn, A. Koka, S. Kurzenhäuser, W. Arnold, "Calibration and Evaluation of Nonlinear Ultrasonic Transmission Measurements on Thin Bonded Interfaces", 7th European Adhesion Conference EURADH 2004, Freiburg, Germany, 5.-9.9.2004, in "Adhesion – Current Research and Applications", Ed. Wulff Possart, WILEY-VCH, Weinheim, Berlin, 2005, 403-419.

S. Hirsekorn, "The Spectral Analysis of a PM Space Unit in the Context of the Classification of Nonlinear Phenomena in Ultrasonic Wave Propagation", in "The universality of nonclassical nonlinearity, with applications to NDE and Ultrasonics", Ed. P.P. Delsanto, Springer, New York, 2005 (in print).

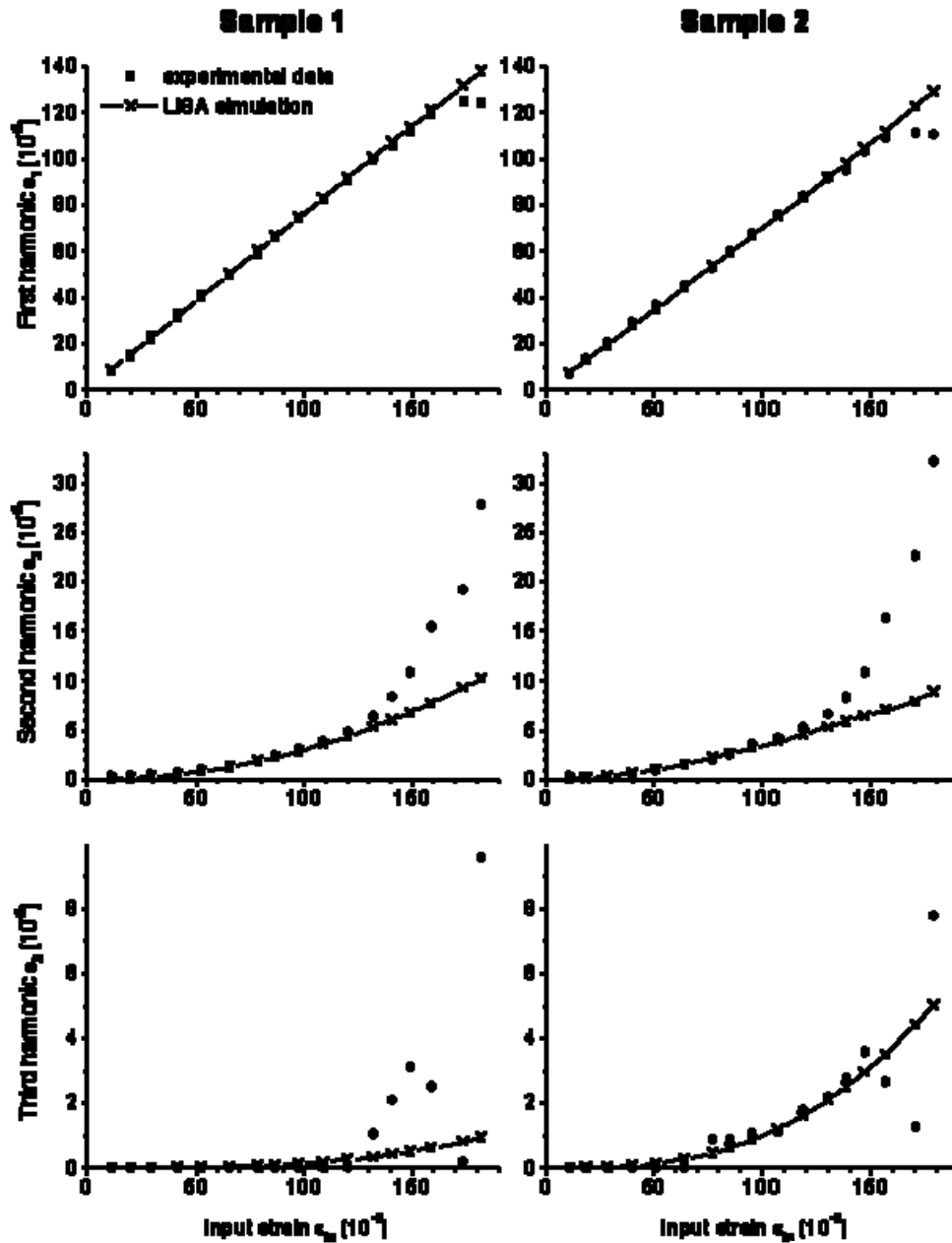


Figure 2.2. Experimental (●) and numerical (x) strain amplitudes of the first three harmonics of the transmitted wave.

by a discussion of the results in relation to frequency spectra of ultrasonic signals measured in transmission through bonds. In general, the analytically calculated results show that the response of a sinusoidally excited rectangular as well as rhombic hysteretic mesoscopic elastic unit (HMEU) contains the incident frequency, all of its higher harmonics, and a static part changing the mean interface width during insonification. The amplitudes ε_n as well as the phases φ_n of the transmitted waves depend on the excitation amplitude as well as on the parameters of the opening and closure process. To obtain the

forces acting in a interstice result the transmitted waves with correct amplitudes and phase factors have to be added up.

In the hysteretic region numerical simulations of the experiments have to take into account explicitly the phases of the transmitted waves. Further, 2D (or even 3D) simulation models including compressional and shear modes and mode conversion are required to describe and evaluate oblique sound incidence onto the interface and/or the transmission of transverse waves.

In ultrasonic transmission measurements small variations in sample thickness will cause only small differences in the amplitudes of the transmitted waves, but might cause significant changes in the phases. If the excitation signals are tone bursts of about 14 to 30 cycles, as it is the case when higher harmonics generation is investigated, the signals transmitted through thin samples consist of the superposition of forward and backward reflected waves. Then, significant changes in the phases might cause also significant variations in the amplitude spectra of the detected signals. This is considered in detail in the context of the output signal calibration in the 1D case. The problem will increase for oblique sound incidence including mode conversion, especially in complex geometrical structures in which waves reflected from several different edges may superpose.

In this respect, virtual experiments will be performed in the near future on complex objects alike those proposed in the minutes of the Torino meeting, Jan 26-27, 2006, but containing bonds which might have weak regions (see Figure 2.3). Simulations shall be carried out using the 2D and/or 3D numerical codes developed in WP2. The output signal shall be analysed concerning amplitudes and phases of the transmitted waves. Changes in the results due to local thickness variations of the sample shall be investigated. For thick bonds (thickness of the same order of magnitude or larger than the wave lengths of the ultrasonic waves) also investigations concerning local variations in the thickness of the interface layer are required.

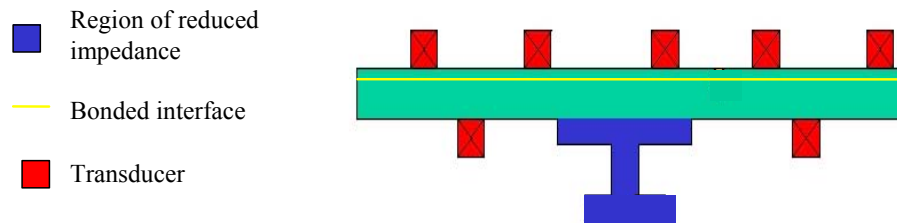


Figure 2.3 : Possible virtual experimental set up to simulate a complex object with a bond (in close relation with the virtual experiment in time reversal acoustics). The bond might have weak region. The different transducers might be used as trasmitters as well as receivers.

D7.3 imaging using the vibro-acoustics methods

The ultrasonic modulation technique currently being developed at Bristol is global, but the high frequencies used and some initial experimental results suggested that the technique could be developed to provide localisation. The use of continuous signals for excitation lead to the excitation of resonances in the sample. A 3D finite element model of the geometrically simplest experimental system was used to give an insight into the shape the modes associated with these resonances. At the frequencies considered (100-500kHz) both the model and experiments indicated that there were many modes separated only by small frequency differences. The model demonstrated that even over small changes in frequency there were significant variations in mode shape and that the modes were, in general poorly localised. This suggested that a straightforward method of localisation would not be possible with continuous excitation. The importance of mode to the energy at the damage and the resulting variation in non-linear response resulted in the implementation of the multi-mode approach described in WP1-D4. It was suggested that information from degree of non-linearity generated by excitation at each mode, along with the mode-shapes could be used to give localisation information, however a sufficiently accurate model was not developed to test this approach.